Electron paramagnetic resonance investigation of photosynthetic reaction centers from *Rhodobacter sphaeroides* R-26 in which Fe^{2+} was replaced by Cu^{2+}

Determination of hyperfine interactions and exchange and dipole–dipole interactions between Cu^{2+} and Q$_A^-$

R. Calvo,* M. C. G. Passeggi,* R. A. Isaacson,‡ M. Y. Okamura,‡ and G. Feher‡

*INTEC (Consejo Nacional de Investigaciones Científicas y Técnicas and Universidad Nacional del Litoral), Guemes 3450, 3000 Santa Fe, Argentina; and ‡Department of Physics, University of California at San Diego, La Jolla, California 92093 USA

ABSTRACT   We report electron paramagnetic resonance (EPR) experiments in frozen solutions of unreduced and reduced photosynthetic reaction centers (RCs) from *Rhodobacter sphaeroides* R-26 in which Fe^{2+} has been chemically replaced by the isotope ^{65}Cu^{2+}. Samples in which the primary quinone acceptor Q$_A$ is unreduced (Cu^{2+}Q$_A$:RCs) give a powder EPR spectrum typical for Cu^{2+} having axial symmetry, corresponding to a $d(x^2 - y^2)$ ground state orbital, with g values $g_\| = 2.314 \pm 0.001$ and $g_\perp = 2.060 \pm 0.003$. The spectrum shows a hyperfine structure for the nuclear spin of copper ($^{65}I = 3/2$) with $A_\| = (-167 \pm 1) \times 10^{-4}$ cm^{-1} and $|A_\perp| = (16 \pm 2) \times 10^{-4}$ cm^{-1}, and hyperfine couplings with three nitrogen ligands. This has been verified in samples containing the naturally occurring ^{14}N isotope ($I = 1$), and in samples where the nitrogen ligands to copper were replaced by the isotope ^{15}N ($I = 1/2$). We introduce a model for the electronic structure at the position of the metal ion which reflects the recently determined three-dimensional structure of the RCs of *Rb. sphaeroides* (Allen, J. P., G. Feher, T. O. Yeates, H. Komiya, and D. C. Rees. 1987. *Proc. Natl. Acad. Sci. USA*. 84:5730; Allen, J. P., G. Feher, T. O. Yeates, H. Komiya, and D. C. Rees. 1988. *Proc. Natl. Acad. Sci. USA*. 85:8487) as well as our EPR results. In this model the copper ion is octahedrally coordinated to three nitrogens from histidine residues and to one carboxylate oxygen from a glutamic acid, forming a distorted square in the plane of the $d(x^2 - y^2)$ ground state orbital. It is also bound to a nitrogen of another histidine and to the other carboxylate oxygen of the same glutamic acid residue, in a direction approximately normal to this plane.

The EPR spectrum changes drastically when the quinone acceptor Q$_A$ is chemically reduced (Cu^{2+}Q$_A^-$:RCs); the change is due to the exchange and dipole–dipole interactions between the Cu^{2+} and Q$_A^-$ spins. A model spin Hamiltonian proposed for this exchange coupled copper-quinone spin dimer accounts well for the observed spectra. From a comparison of the EPR spectra of the Cu^{2+}Q$_A$:RC and Cu^{2+}Q$_A^-$:RC complexes we obtain the values $|J_0| = (0.30 \pm 0.02)$ K for the isotropic exchange coupling, and $|d| = (0.010 \pm 0.002)$ K for the projection of the dipole–dipole interaction tensor on the symmetry axis of the copper spin. From the EPR experiments only the relative signs of J_0 and d can be deduced; it was determined that they have the same sign. The magnitude of the exchange coupling calculated for Cu^{2+}Q$_A^-$:RC is similar to that observed for the Fe^{2+}Q$_A^-$:RC complex ($J_0 = -0.43$ K). The exchange coupling is discussed in terms of the superexchange paths connecting the Cu^{2+} ion and the quinone radical using the structural data for the RCs of *Rb. sphaeroides*. From the value of the dipole–dipole interaction, d, we determined $R \approx 8.4$ Å for the weighted distance between the metal ion and the quinone in reduced RCs, which is to be compared with 10 Å obtained from x-ray analysis of unreduced RCs. This points to a shortening of the Cu^{2+} − Q$_A^-$ distance upon reduction of the quinone, as has been proposed by Allen et al. (1988).

INTRODUCTION

Electron paramagnetic resonance (EPR) is a powerful technique to study metal ions in metalloproteins (Brill, 1977; Solomon et al., 1983). It provides information about the electronic structure of the metal and its surroundings, including the geometry and nature of the ligands. This information is complementary to the three dimensional structure of the protein determined by x-rays.

EPR studies of metal ions interacting with paramagnetic free radicals provide information about the magnetic interactions (exchange and dipole–dipole) between them. The magnitude of the exchange interaction between unpaired spins in proteins provides information about the electronic paths connecting these spins. It has

been proposed that the matrix elements responsible for superexchange (Anderson, 1959; Hay et al., 1975) are related to those for electron transfer (Okamura et al., 1979; Okamura and Feher, 1989; DeVault, 1984). Thus, the study of superexchange interactions is of particular interest in proteins in which electron transfer processes between paramagnetic species takes place.

The magnitude of the dipole–dipole interaction allows one to calculate the distance between the interacting spins and also allows the determination of conformational changes produced during the functional cycle of the protein.

EPR has played an important role in the understanding of the electronic structure of bacterial photosynthetic

reaction centers (RCs). Together with the electron nuclear double resonance technique it has been applied to the identification and characterization of the primary donors and acceptors (reviewed by Hoff, 1979, 1987) and has provided key pieces of information about many aspects of the structure and function of the RCs (Okamura et al., 1975; Feher and Okamura, 1978; Okamura et al., 1982).

EPR measurements on the reduced acceptor $Fe^{2+}Q_A^-$: RC complex of *Rhodobacter sphaeroides* and *Rhodobacter viridis* have been reported by McElroy et al. (1970), Feher (1971), Leigh and Dutton (1972), and Dutton et al. (1973). The broad EPR signal observed at cryogenic temperatures, centered at $g \approx 1.8$ with wings extending from $g \approx 5$ to $g < 0.8$, was attributed to the reduced primary acceptor. A detailed interpretation of these results was given by Butler et al. (1984), who studied frozen solutions of RCs from *Rb. sphaeroides*. To explain the data they assumed that the signal arises from the spin $S_Q = \frac{1}{2}$ of the reduced quinone Q_A^-, interacting with the spin $S_{Fe} = 2$ of the Fe^{2+} ion. Using a model based on a spin Hamiltonian containing the exchange interaction, $\vec{J}$, of the form:

$$- \vec{S}_Q \cdot \vec{J} \cdot \vec{S}_{Fe},$$

they evaluated the principal components of the $\vec{J}$ tensor. The values $J_x = -0.13$ K, $J_y = -0.58$ K, and $J_z = -0.58$ K, giving an isotropic antiferromagnetic exchange interaction of $J_0 = -0.43$ K, explained well the data obtained in frozen solutions (Butler et al., 1984). The analysis of the EPR data was supported by previous magnetic susceptibility measurements on unreduced and reduced RCs (Butler et al., 1980).

Dismukes et al. (1984) reported EPR measurements on the iron-semiquinone acceptor in partially oriented whole cells and chromatophores of *Rb. viridis*. To interpret the data they assumed an isotropic exchange interaction of magnitude $|J_0| = 0.12$ K. These authors observed a selective broadening of some of the EPR lines which they attributed to an exchange narrowed dipole–dipole interaction.[1]

Recently, EPR studies of the reduced iron-quinone complex in single crystals of RCs from *Rb. viridis* (Evelo et al., 1988; Gast et al., 1989) and from *Rb. sphaeroides*

(Allen et al., 1989), were reported. These experiments on single crystals should provide complete information about the magnetic interactions (exchange and dipole–dipole couplings) between Fe^{2+} and Q_A^-. However, the observed broadening of the EPR line, attributed to a dispersion of the values of the crystal field parameters of Fe^{2+}, has made a detailed analysis difficult so far.

The electronic structure of Fe^{2+} in RCs of *Rb. sphaeroides* has been studied by other techniques, including Mössbauer spectroscopy (Debrunner et al., 1975; Boso et al., 1981), magnetic susceptibility (Butler et al., 1980), and Extended X-ray Absorption of Fine Structure Studies (Bunker et al., 1982; Eisenberger et al., 1982). The electronic structure of Fe^{2+} is determined by the six electrons in the unfilled d-shell. They give rise to 210 electronic states,[2] five of which are split off to form the ground state manifold. These are the states of interest for magnetic properties because they are the only ones that are significantly populated at room temperature. Fe^{2+} is a non-Kramers' ion with $S_{Fe} = 2$; it is EPR silent, and is detectable by EPR only through the effect it produces on other magnetic species (for example, Q_A^-, with $S_Q = \frac{1}{2}$). In addition, because Fe^{2+} is a fast relaxer, it changes drastically the relaxation times of other coupled magnetic species (e.g., Q_A^-; Calvo et al., 1982), giving rise to changes of the EPR spectra at higher temperatures.

The Fe^{2+} ion can be extracted from the RC and replaced by other divalent ions such as Co^{2+}, Ni^{2+}, Cu^{2+}, Mn^{2+}, Zn^{2+}, and Fe^{2+} (Debus et al., 1986). The electron transfer characteristics of the iron depleted samples reconstituted with these ions are essentially the same as those of native RCs. The possibility of such replacement allows one to use other spin probes to study the electronic structure of the RC in the neighborhood of the metal site, and the magnetic interactions between the metal ion and the quinone radical. The simplest magnetic system is obtained when iron is replaced by copper, which has one hole in the unfilled d-shell (3 d^9). EPR studies of Cu^{2+}:RC are conceptually simpler than in Fe^{2+}:RC. Copper can be detected in samples in which the primary quinone Q_A is unreduced ($Cu^{2+}Q_A$:RC), as well as in those where it is reduced ($Cu^{2+}Q_A^-$:RC). It has effectively one unpaired electron with an effective spin $S_{Cu} = \frac{1}{2}$. In unreduced samples the EPR spectrum provides information about the symmetry of the metal site and the nature of the ligands (Abragam and Bleaney, 1970; Zeiger and Pratt, 1973). Furthermore, the interaction of the unpaired electron with the nuclear spins of the copper and the ligands, gives rise to hyperfine splittings, providing additional information about the system.

---

[1]We believe that this interpretation is incorrect. The exchange narrowing process invoked in Appendix D of the paper by Dismukes et al. (1984) results from exchange interactions in a system involving a large number of spins where random spin exchange fluctuations average out the dipolar broadening (Anderson and Weiss, 1953; Anderson, 1954). For a system of two spins (e.g., $Fe^{2+}Q^-$ or $Cu^{2+}Q^-$ magnetically diluted in a diamagnetic protein matrix) the combined effect of exchange interactions can be calculated by standard spin-Hamiltonian methods as is done in this paper, e.g., Eq. 17.

---

[2]This is the number of ways that six electrons can be distributed over 10 orbitals, i.e., $10!/6!4!$

Feher et al. (1986) reported EPR data on frozen solutions of unreduced RCs in which the Fe^{2+} was chemically replaced by Cu^{2+}. The EPR spectra were interpreted as arising from Cu^{2+} in an axially distorted octahedral site; hyperfine splittings due to the interaction with the copper nucleus and with the nuclei of three nitrogen ligands were observed. Buchanan and Dismukes (1987) reported EPR experiments in unreduced RCs from *Rb. sphaeroides* (strain Y) in which the iron ion was biosynthetically replaced by Cu^{2+} during the growth of the cells. Their results differed from those reported earlier (Feher et al., 1986). They obtained different g values and copper hyperfine parameters, and most importantly, they showed well resolved hyperfine couplings with four nitrogen ligands.

In this work a detailed study of the EPR spectra of frozen solutions of unreduced RCs ($Cu^{2+}Q_A$:RCs) and reduced RCs ($Cu^{2+}Q_A^-$:RCs) have been performed. Our results on $Cu^{2+}Q_A$:RC are similar but more detailed than those reported by Feher et al. (1986). The results are analyzed in terms of the now available three-dimensional structure of the RC in the vicinity of the metal ion (Allen et al., 1987, 1988). The differences between our EPR data and those reported by Buchanan and Dismukes (1987) are discussed.

The EPR data obtained in samples, where Q_A was chemically reduced ($Cu^{2+}Q_A^-$:RC) are used to evaluate the magnitudes of the exchange and dipole–dipole interactions between the copper and quinone spins; the structural implications of these values are discussed. A preliminary account of this work has been reported (Calvo et al., 1990).

MATERIALS AND METHODS

Reaction centers

Reaction centers of *Rb. sphaeroides* R-26 were prepared by the procedure of Feher and Okamura (1978), as modified by Debus (1985). The Fe^{2+} was replaced with $^{65}Cu^{2+}$ by chemical methods, as described by Debus et al. (1986). In summary, this treatment involves removal of Fe^{2+} by incubation with LiSCN and o-phenanthroline. The Fe free RCs were purified to remove denatured LM complexes (RCs without the H subunit), and Cu^{2+} was added back. The excess Cu^{2+} was removed by dialysis. The metal content of the RCs was 0.8 Cu/RC and (0.1–0.3) Fe/RC. To simplify the interpretation of the EPR data we used Cu^{2+} enriched 99% with the ^{65}Cu isotope.

The chemical reduction of the $Cu^{2+}Q_A$:RCs was accomplished by the addition of dithionite (50 mM) before freezing. The RC concentration was 0.14 mM ($A_{802}^{1 cm} = 40$). Samples of ~0.5 ml were frozen in Rexolite tubes having an inside diameter of 8 mm, appropriate to the microwave cavity. All samples were stored at 77 K.

The ^{15}N enriched reaction centers were obtained by growing the bacteria in a synthetic Hutner medium, supplemented by 0.5 g/l of 99% ^{15}N enriched ammonium acetate, as the sole nitrogen source.
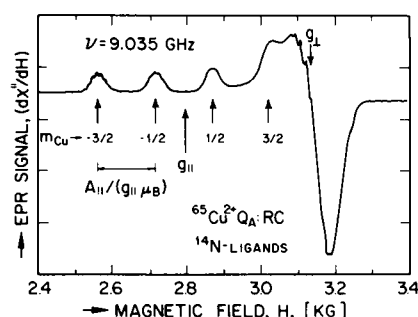

FIGURE 1   EPR spectrum of a frozen solution of unreduced $^{65}Cu^{2+}Q_A$: RC. Experimental conditions: $H_{mod} = 5$ G ptp, 90 Hz, $T = 77$ K, $\nu = 9.0354$ GHz, 100 field sweeps of 1 min each. The resonance peaks are identified by the quantum number m_{Cu} of the nuclear spin of copper. The field positions associated with the values of $g_\parallel$ and $g_\perp$ are indicated. The value of $A_\parallel$ is assumed to be negative in labeling the resonances. The structures observed on the $m_{Cu} = -\frac{3}{2}$ and $-\frac{1}{2}$ lines are due to superhyperfine interaction with the nitrogen ligands; shown in more detail in the expanded traces of Fig. 2 and 3.

EPR experiments

EPR spectra were obtained on a 9-GHz superheterodyne spectrometer of local design (Feher, 1957; McElroy et al., 1974; Butler et al., 1984). The field derivative of the spectra was obtained with low frequency field modulation ($\approx$90 Hz), and phase sensitive detection of the signal. To improve the signal-to-noise ratio of the EPR spectra many field sweeps were averaged and stored in a Nicolet Instruments 1180 minicomputer (Madison, WI).

Computer calculations

We used existing methods and software to simulate the EPR spectra (Belford and Nilges, 1979; Rothenberger, 1988). The computer program was furnished by the Illinois Electron Spin Resonance Research Center, (Urbana, IL) National Institutes of Health Division of Research Resources grant No. RR01811. The program generates, for a given set of spin-Hamiltonian parameters, the powder spectrum for an electronic spin ½ ion interacting with its own nucleus, and with up to three ligand nuclei. It performs a matrix diagonalization of the Zeeman and hyperfine interactions; the ligand hyperfine couplings are treated as a perturbation.

EXPERIMENTAL RESULTS

Unreduced $Cu^{2+}Q_A$:RCs

Fig. 1 displays the EPR spectrum of a frozen solution of $Cu^{2+}Q_A$:RCs, observed at 77 K, and at a microwave frequency of ~9 GHz. Four equally spaced EPR peaks are observed at low magnetic field. They are attributed to the hyperfine coupling of the unpaired spin of the Cu^{2+} with the nuclear spin of ^{65}Cu.[3] The two lowest field lines exhibit

---

[3]Copper has two natural isotopes, 63 and 65, having both $I = \frac{3}{2}$ and magnetic moments differing by ~7%. To simplify the analysis of the EPR spectra, the RCs were enriched 99% with the isotope ^{65}Cu.

a multiline structure described below. In addition, a stronger peak is observed at a higher magnetic field. As discussed later, the spectrum is typical of Cu^{2+} in an axially symmetric ligand field.

The lowest field peak of the spectrum of Fig. 1 is displayed in greater detail in Fig. 2. Seven equally spaced peaks with a splitting of 10.5 G and with relative amplitude ratios of ~1:3:6:7:6:3:1 are observed. As discussed later, this structure is attributed to a hyperfine coupling between the spin of the unpaired electron of Cu^{2+} with the nuclear spins of three nitrogen ligands of the 99.6% abundant ^{14}N isotope ($^{14}I = 1$). To prove this hypothesis, we measured the EPR spectrum of a $Cu^{2+}Q_A$: RC sample in which the nitrogen ligands to copper were 99% enriched with the ^{15}N isotope ($^{15}I = \frac{1}{2}$). The overall spectrum of this sample is similar to that shown in Fig. 1, except for the structure of the two lowest field lines. The lowest field peak of this spectrum is displayed in Fig. 3. Four peaks, with amplitude ratios of ~1:3:3:1 and splittings of 14.6 G are observed.

A portion of the high field peak of the spectrum of Fig. 1, shows some ligand hyperfine structure. The splittings are ~14 G but the resolution is not good enough to determine the total number of peaks.

Reduced $Cu^{2+}Q_A^-$:RCs

The EPR spectrum of $Cu^{2+}Q_A^-$:RCs (produced by chemical reduction with dithionite) is shown in Fig. 4. This spectrum is very different from that obtained in unreduced samples, displayed in Fig. 1. The low field peaks moved toward higher magnetic fields; the number of peaks is larger than before, but no ligand hyperfine structure is observed. To display a more detailed view of
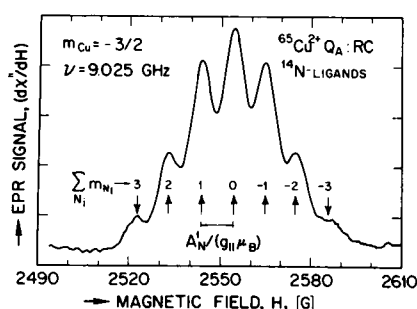
FIGURE 2 Expanded trace of the low field peak $m_{Cu} = -\frac{3}{2}$ of $Cu^{2+}Q_A$:RC of Fig. 1, showing the details of the ^{14}N ligand hyperfine splitting ($^{14}I_N = 1$). In labeling the resonances with $\Sigma_{N_i} m_{N_i}$, where m_{N_i} is the nuclear spin quantum number of each nitrogen ligand N_i, we assumed that $A_N^I > 0$. Experimental conditions as in Fig. 1 except for the amplitude and rates of the field sweep (100 G/min). The lower resolution of this structure in Fig. 1 is due to the faster sweep rate of the magnetic field (1,000 G/min).
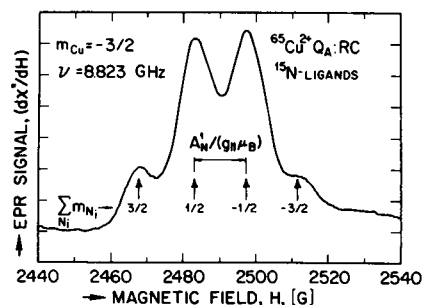
FIGURE 3 Expanded trace of the low field peak $m_{Cu} = -\frac{3}{2}$ of the EPR spectrum of the $^{65}Cu^{2+}Q_A$:RC sample in which the nitrogens were replaced by the ^{15}N isotope ($^{15}I_N = \frac{1}{2}$). Experimental conditions as in Fig. 2, except $\nu = 8.823$ GHz.

the peaks, a portion of the spectrum of Fig. 4 is shown enlarged in Fig. 5 a.

ANALYSIS AND INTERPRETATION OF THE DATA ON $Cu^{2+}Q_A$:RCs

The spin Hamiltonian based on a molecular model

The EPR spectra of Cu^{2+} ions can be described by the spin Hamiltonian (Abragam and Bleaney, 1970):

$$H_{Cu} = \mu_B \vec{H} \cdot \vec{g}_{Cu} \cdot \vec{S}_{Cu} + \vec{S}_{Cu} \cdot \vec{A}_{Cu} \cdot \vec{I}_{Cu}$$
$$+ \sum_{N_i} \vec{S}_{Cu} \cdot \vec{A}_{N_i} \cdot \vec{I}_{N_i}, \quad (1)$$

where $\vec{S}_{Cu}$ is the effective electronic spin of copper ($S_{Cu} = \frac{1}{2}$), $\vec{I}_{Cu}$ is its nuclear spin ($^{65}I_{Cu} = \frac{3}{2}$), and μ_B is the Bohr magneton. The g tensor and copper hyperfine tensor $\vec{g}_{Cu}$ and $\vec{A}_{Cu}$ give the strength of the coupling of $\vec{S}_{Cu}$ with the
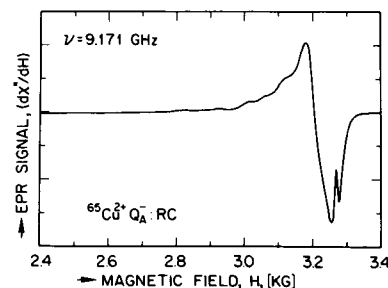
FIGURE 4 EPR spectrum of the $^{65}Cu^{2+}Q_A^-$:RC sample obtained by chemical reduction with dithionite of the $^{65}Cu^{2+}Q_A$:RC sample that produced the spectrum of Fig. 1. Note the drastic change of the spectrum from that obtained from the unreduced sample, shown in Fig. 1.
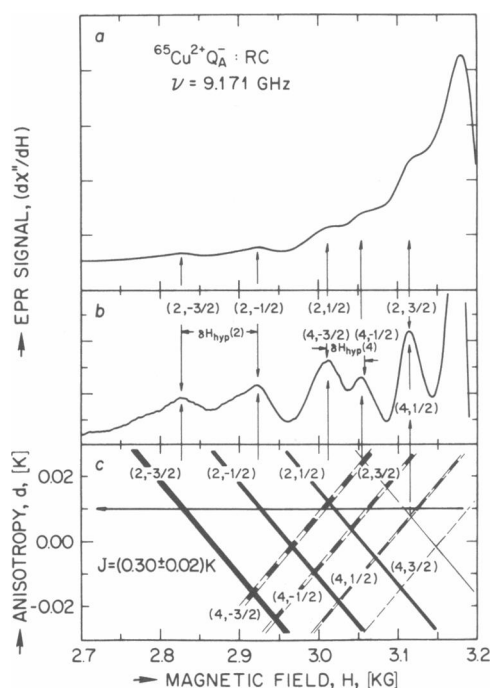
FIGURE 5 Comparison of expanded spectrum of Fig. 4 with the theoretically predicted spectrum. (a) Expanded trace of the spectrum shown in Fig. 4. (b) Enlarged spectrum shown in a, in which a background simulated by an arbitrary fitting function $f(H) = C_1 + C_2(H - C_3)^5$, has been subtracted. Arrows indicate the position and assignments of the peaks. (c) Positions $H_{2,m}$ and $H_{4,m}$ of the resonances calculated from Eqs. 17 b and d for $J_0 = -(0.30 \pm 0.02)$ K, as a function of the anisotropy parameter d. Solid lines correspond to the positions of the $H_{2,m}$ group; dashed lines are those obtained for the $H_{4,m}$ group. The width of the lines represent the uncertainties in J_0 (± 0.02K). Horizontal arrow in c corresponds to the value $d = 0.010$ K that best reproduces the positions of the observed peaks.

applied magnetic field $\vec{H}$, and with the nuclear magnetic moment associated with $\vec{I}_{Cu}$, respectively. The last term in Eq. 1 is the ligand hyperfine (superhyperfine) interaction due to the coupling of $\vec{S}_{Cu}$ with the nuclear spins $\vec{I}_{N_i}$ of the nitrogen ligands ($I_N = 1$ for ^{14}N and $I_N = \frac{1}{2}$ for ^{15}N). This interaction gives rise to the multiline structure of the resonances (Figs. 1–3). The index i refers to the different nitrogens that form ligands to the Cu.

The first (Zeeman) term of Eq. 1 is larger than the hyperfine interactions; we can, therefore, neglect higher order perturbation terms and write the Hamiltonian of Eq. 1 for an arbitrary orientation $\hat{h} = \vec{H}/|\vec{H}|$ of the applied magnetic field as (Abragam and Bleaney, 1970):

$$H_{Cu} = g_{Cu}\mu_B H S^h_{Cu} + \alpha_{Cu}S^h_{Cu}I^h_{Cu} + \sum_{N_i} \alpha_{N_i}S^h_{Cu}I^h_{N_i}, \quad (2)$$

where S^h_{Cu}, I^h_{Cu}, and I^h_N are the projections along $\hat{h}$ of $\vec{S}_{Cu}, \vec{I}_{Cu}, \vec{I}_N$, and $g^2_{Cu} = \hat{h} \cdot (\vec{g}_{Cu} \cdot \vec{g}_{Cu}) \cdot \hat{h}; g^2_{Cu}\alpha^2_{Cu} = \hat{h} \cdot (\vec{g}_{Cu} \cdot \vec{A}_{Cu} \cdot \vec{A}_{Cu} \cdot \vec{g}_{Cu}) \cdot \hat{h}$ and $g^2_{Cu}\alpha^2_N = \hat{h} \cdot (\vec{g}_{Cu} \cdot$

$\vec{A}_N \cdot \vec{A}_N \cdot \vec{g}_{Cu}) \cdot \hat{h}$ are the projections of the tensors $(\vec{g}_{Cu} \cdot \vec{g}_{Cu}); (\vec{g}_{Cu} \cdot \vec{A}_{Cu} \cdot \vec{A}_{Cu} \cdot \vec{g}_{Cu})$ and $(\vec{g}_{Cu} \cdot \vec{A}_N \cdot \vec{A}_N \cdot \vec{g}_{Cu})$ along $\hat{h}$. Indicating by m_{Cu} and m_{N_i} the possible values of I^h_{Cu} and $I^h_{N_i}$, the position of the magnetic field at resonance corresponding to (m_{Cu}, m_{N_i}), it is obtained from Eq. 2:

$$H(m_{Cu}, m_{N_i}) = H_0 - [\alpha_{Cu}(\hat{h})/(g_{Cu}\mu_B)]m_{Cu}$$
$$- \sum_{N_i} [\alpha_{N_i}(\hat{h})/(g_{Cu}\mu_B)] \, m_{N_i}, \quad (3)$$

where $m_{Cu} = \frac{3}{2}, \frac{1}{2}, -\frac{1}{2}, -\frac{3}{2}$, and $m_N = 1, 0, -1$ for ^{14}N or $m_N = \frac{1}{2}, -\frac{1}{2}$ for ^{15}N, for each nitrogen ligand. The central field of the spectrum is at $H_0 = h\nu/(g_{Cu}\mu_B)$, where ν is the microwave frequency. The observed splittings in an applied magnetic field $\vec{H}$, due to the hyperfine interactions of $\vec{S}_{Cu}$ with $\vec{I}_{Cu}$ and with $\vec{I}_{N_i}$ are given by $\alpha_{Cu}(\hat{h})/(g_{Cu}\mu_B)$ and $\alpha_{N_i}(\hat{h})/(g_{Cu}\mu_B)$. When the projections along $\hat{h}$ of the hyperfine coupling tensors $\vec{A}_{Cu}$ and $\vec{A}_{N_i}$ are negative, $\alpha_{Cu}(\hat{h})$ and $\alpha_{N_i}(\hat{h})$ have to be taken negative to obtain the right labeling of the resonances.

Let us consider the simple case of four equivalent nitrogen ligands around copper, forming a square planar complex in the xy plane. The point symmetry of copper would be C_{4h} or higher (Cotton, 1963), i.e., there is a four-fold symmetry axis and a mirror plane perpendicular to it. In this case, the tensors $\vec{g}_{Cu}, \vec{A}_{Cu}$, and $\vec{A}_{N_i}$ may be expressed in diagonal form in the same basis of eigenvectors. The $\hat{z}$ (principal) axis will be along the C_4 axis, and the $\hat{x}$ and $\hat{y}$ axes will be in a plane perpendicular to it, i.e., in the directions of the Cu-N bonds. The tensors $\vec{g}_{Cu}$ and $\vec{A}_{Cu}$ have axial symmetry, with $g_\parallel$ and $A_\parallel$ along the $\hat{z}$ axis (called the "parallel" direction), and $g_\perp$ and $A_\perp$ in the xy plane (perpendicular direction). The principal components of the N hyperfine tensors are denoted by superscripts; along the Cu-N sigma bond by A^3_N, along the $\hat{z}$ direction by A^1_N and along the third orthogonal direction by A^2_N. From symmetry considerations A^1_N, A^2_N, and A^3_N are the same for all nitrogens in the plane. Experimental data obtained on copper-amino acid complexes with N ligands indicate that $A^1_N \approx A^2_N < A^3_N$. This relation is approximately valid even when the four-fold symmetry around the Cu^{2+} ion does not exactly hold (Schweiger, 1982). Furthermore, the symmetry of the ligand hyperfine tensors described above would be approximately valid if there are only three nitrogen ligands, with the fourth position in the square occupied by an oxygen atom ($I = 0$ for ^{16}O). This situation is schematically shown in Fig. 6. As we shall see later, this simplified representation of the problem represents a good approximation of the molecular cluster around Cu^{2+} discussed in this paper.

The EPR spectrum displayed in Fig. 1 corresponds to a frozen solution of $Cu^{2+}Q_A$:RCs in which all protein orientations are present. Descriptions of EPR spectra of
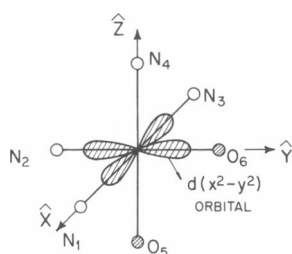
FIGURE 6 Schematic representation of the proposed bonding scheme for Cu^{2+} with its ligands. The Cu^{2+} ion has three nitrogen and one oxygen ligand in the plane of the $d(x^2 - y^2)$ ground state orbital (*dashed lines*), and one nitrogen and one oxygen ligand in the apical positions. The spectra shown in Figs. 2 and 3 correspond to the magnetic field along the parallel ($\hat{z}$) direction.

randomly oriented copper complexes (powder samples) have been discussed by several authors (see for example, Abragam and Bleaney, 1970; Solomon et al., 1983); we shall briefly summarize the pertinent ideas involved. When the gyromagnetic tensor has axial symmetry, as for Cu^{2+} with $d(x^2 - y^2)$ or $d(z^2)$ ground state orbitals, the EPR spectrum of a powder sample is limited by the magnetic fields corresponding to the values of $g_z = g_\parallel$ and $g_x = g_y = g_\perp$, with peaks observed at these values. This behavior is accentuated by the standard experimental procedure of taking the field derivative of the EPR spectrum. Because the perpendicular plane covers a wider solid angle than the parallel direction, the EPR signal exhibits a stronger peak at $g \approx g_\perp$, than at $g \approx g_\parallel$. This situation remains essentially unchanged when g is slightly anisotropic in the perpendicular plane, i.e., when $g_x \neq g_y$ but $|g_x - g_y| \ll |g_\parallel - g_\perp|$, where $g_\perp = \frac{1}{2}(g_x + g_y)$. The main effect of this anisotropy is a broadening of the peak corresponding to the perpendicular direction. Thus, in a first approach to the analysis of the spectra, only signals arising from Cu^{2+} ions with $\vec{H}$ along the parallel or along the perpendicular directions are detectable. With $\vec{H}$ along the parallel (i.e., $\hat{z}$) direction, $\alpha_{Cu}(\hat{h}) = A_\parallel$ and $\alpha_{N_i}(\hat{h}) = A_N^i$ for all ligands N_i and Eq. 3 can be written as

$$H(m_{Cu}, m_{N_i}) = H_0 - [A_\parallel/(g_\parallel \mu_B)]\, m_{Cu}$$
$$- [A_N^i/(g_\parallel \mu_B)] \sum_{N_i} m_{N_i}, \quad (4)$$

where $H_0 = h\nu/(g_\parallel \mu_B)$.

The spectrum of Fig. 1 shows a group of four peaks spaced by 154 G which are attributed to copper centers with the magnetic field applied along the parallel direction ($g_\parallel$). The fourth peak of this group overlaps with the strong peak observed at high field. The low field quartet in Fig. 1 displays the ligand (^{14}N) hyperfine structure with decreasing resolution on going from the lowest field peak ($m_{Cu} = -\frac{3}{2}$) to the higher field peaks. The loss of

resolution of the higher field peaks can be explained by the theory of Froncisz and Hyde (1980) (see also Hyde and Froncisz, 1982). This theory proposes a dispersion of the values of the g factor and the copper hyperfine coupling tensor, which broadens the resonance lines. Because the values of the g factor and the copper hyperfine coupling parameter are a consequence of the same physical mechanism (Maki and McGarvey, 1958a,b; Zeiger and Pratt, 1973), their dispersions are correlated. Consequently, the broadening produced by the dispersion of g adds to or cancels that produced by the dispersion of the hyperfine coupling, depending on the resonance involved.

For a set of n identical ligand nuclei one expects $(2nI + 1)$ hyperfine lines. The observed number of lines for ^{14}N ($I = 1$) is 7 and for ^{15}N ($I = \frac{1}{2}$) it is 4, corresponding to three nitrogens. The expected amplitude ratios of the hyperfine lines are 1:3:6:7:6:3:1 for ^{14}N and 1:3:3:1 for ^{14}N, are given by the multiplicity of the possible values of $\Sigma_{N_i}\, m_{N_i}$ in Eq. 4. These ratios are in good agreement with the values obtained from Fig. 2 (for ^{14}N) and from Fig. 3 (for ^{15}N).

Fig. 6 shows the proposed distribution of the nearest ligands to copper including the position of the $d(x^2 - y^2)$ ground state orbital. There is a significant spin density of the $d(x^2 - y^2)$ ground state orbital at the three nitrogens N_1, N_2, N_3 which gives rise to the observed ligand hyperfine structure. In contrast, the spin density at the position of N_4 is small. Consequently, no resolved hyperfine structure is expected from this nitrogen. The oxygens O_5 and O_6 are nonmagnetic. We shall later discuss this simplified version of the molecular structure around copper in terms of the three-dimensional structure of the RC.

Determination of $g_\parallel$, $g_\perp$, $A_\parallel$, $A_\perp$ and the superhyperfine interaction with the N ligands

The analysis of the low field region of the spectrum of Fig. 1 using Eq. 4 gives:

$$g_\parallel = 2.314 \pm 0.001 \quad \text{and} \quad A_\parallel = (-167 \pm 1) \times 10^{-4}\, cm^{-1}.$$

To determine the sign of $A_\parallel$ and the correct assignment of the magnetic quantum numbers m_{Cu} of the low field group of four lines in Fig. 1, one has to measure the position of forbidden EPR transitions (Maki and McGarvey, 1958a,b). This has not been done in our study of $Cu^{2+}Q_A$: RCs. However, it is clear from data obtained on other copper compounds with a $d(x^2 - y^2)$ ground orbital that $A_\parallel$ is negative (Maki and McGarvey, 1958a,b) and this sign is assumed here without explicit proof. Using Eq. 4

and the data of Figs. 2 and 3 we obtain,

$$A_N^1 (^{14}N) = (11.3 \pm 0.5) \times 10^{-4} \, cm^{-1},$$

$$A_N^1 (^{15}N) = (15.8 \pm 0.5) \times 10^{-4} \, cm^{-1},$$

for ^{14}N and ^{15}N ligands. The ratio $A_N^1(^{14}N)/A_N^1(^{15}N) = 0.72$ obtained from these results agrees well with the known ratio of the nuclear g factors $g(^{14}N)/g(^{15}N) = 0.71$. From the linewidths of the ligand hyperfine peaks in Fig. 2 we determined an upper limit of $|A_N| \leq 2.5 \times 10^{-4} \, cm^{-1}$ for the unresolved hyperfine coupling of Cu^{2+} with any fourth ^{14}N ligand.

At high fields there is one large peak around $g = 2$ (Fig. 1) showing partially resolved hyperfine structure. The structure is attributed to hyperfine splittings with the copper nucleus as well as with the ligand nitrogens. Because in the perpendicular direction Cu and N hyperfine splittings have similar magnitudes and the structure is not well resolved, $A_\perp$, A_N^2, and A_N^3 cannot be obtained from the position of these peaks. We performed therefore, computer simulations of the spectra to obtain the set of values of the parameters of the spin Hamiltonian of Eq. 1 which best reproduce the spectra of Figs. 1–3. The assumption $A_N^1 = A_N^2$ was used in the calculations. We used existing programs (see Materials and Methods) and obtained a good agreement between experimental and simulated spectra. For the perpendicular direction:

$$g_\perp = 2.060 \pm 0.003, \quad |A_\perp| = (16 \pm 2) \, 10^{-4} \, cm^{-1}$$

$$A_N^3(^{14}N) = (14 \pm 2) \, 10^{-4} \, cm^{-1} \quad and$$

$$A_N^3(^{15}N) = (19 \pm 2) \, 10^{-4} \, cm^{-1}.$$

The values obtained for all the spin Hamiltonian parameters are summarized in Table 1. The sign of $A_\perp$ relative to that of $A_{||}$ can be determined for small Cu^{2+} complexes by EPR experiments in liquid solutions. In this case, the Cu^{2+} complex rotates rapidly and the average isotropic hyperfine interaction $A_{iso} = \frac{1}{2} (A_{||} + 2 A_\perp)$ is measured. From the values of A_{iso} and $A_{||}$, the sign of $A_\perp$ relative to that of $A_{||}$ can be obtained (see e.g., Maki and McGarvey, 1958a,b). Because of the large size of the reaction center, this motional narrowing effect cannot be observed in the $Cu^{2+}Q_A$:RC complex.

Interpretation of the EPR parameters in terms of the electronic structure of $Cu^{2+}Q_A$:RCs

Divalent copper has nine electrons in the three-dimensional shell that behave as a single unpaired hole with $l = 2$ and $s = \frac{1}{2}$. The energy level scheme and the EPR spectra of Cu^{2+} ions has been described by many authors (e.g., Abragam and Bleaney, 1970; Zeiger and Pratt, 1973; Gray and Solomon, 1981; Solomon et al., 1983). In a tetragonally distorted octahedral coordination the lowest level is either a $d(x^2 - y^2)$, for an elongated octahedron, or a $d(z^2)$ orbital for a compressed octahedron.

The values of $g_{||}$, $g_\perp$, $A_{||}$, and $A_\perp$ obtained from the EPR spectra are related to the energies of the copper electronic orbitals in the field of its ligands, and to the value of the spin-orbit interaction λ (Abragam and Bleaney, 1970; Zeiger and Pratt, 1973). When the ground state is a $d(x^2 - y^2)$ orbital one obtains:

$$g_{||} = g_0 - 8 \lambda/\delta_0, \quad (5a)$$

$$g_\perp = g_0 - 2 \lambda/\delta_1. \quad (5b)$$

When the orbital ground state is a $d(z^2)$ one obtains:

$$g_{||} = g_0, \quad (6a)$$

$$g_\perp = g_0 - 6 \lambda/\delta_2, \quad (6b)$$

where g_0 is the free electron g value 2.0023, δ_0, and δ_1 are the energy splittings between the ground state and the states $d(xy)$ and $(d[xz], d[yz])$, respectively, and δ_2 is the energy splitting between the states $(d[xz], d[yz])$ and $d(z^2)$. The value $\lambda = -830 \, cm^{-1}$ for free Cu^{2+} ions was reduced due to covalent bonding of Cu^{2+} with its ligands (Abragam and Bleaney, 1970; Zeiger and Pratt, 1973) to $\lambda = -660 \, cm^{-1}$. Adopting values of $\delta_0 \approx \delta_1 \approx \delta_2 \approx 12,300$ cm^{-1}, as obtained from the optical absorption spectra of aqueous solutions of copper, one obtains for a Cu^{2+} ion with a $d(x^2 - y^2)$ orbital ground state (Eqs. 5a–b):

$$g_{||} \approx 2.4 \quad and \quad g_\perp \approx 2.1,$$

and for a $d(z^2)$ ground orbital state (Eqs. 6a–b):

$$g_{||} \approx 2 \quad and \quad g_\perp \approx 2.3.$$

TABLE 1 Values of the parameters of the spin-Hamiltonian of Eq. 1 obtained from the EPR spectra of Figs. 1–3

$g_{||} = 2.314 \pm 0.001$	$A_{||} = (-167 \pm 1) \, 10^{-4} \, cm^{-1}$
$g_\perp = 2.060 \pm 0.003$	$|A_\perp| = (16 \pm 2) \, 10^{-4} \, cm^{-1}$
$A_N^1(^{14}N) = (11.3 \pm 0.5) \, 10^{-4} \, cm^{-1}$	$A_N^1(^{15}N) = (15.8 \pm 0.5) \, 10^{-4} \, cm^{-1}$
$A_N^2(^{14}N) = (11.3 \pm 0.5) \, 10^{-4} \, cm^{-1}$	$A_N^2(^{15}N) = (15.8 \pm 0.5) \, 10^{-4} \, cm^{-1}$
$A_N^3(^{14}N) = (14 \pm 2) \, 10^{-4} \, cm^{-1}$	$A_N^3(^{15}N) = (19 \pm 2) \, 10^{-4} \, cm^{-1}$

We assume $A_N^1 = A_N^2$.

The experimental values, $g_\parallel = 2.314$ and $g_\perp = 2.060$, show that the lowest unfilled ground state orbital for Cu^{2+} in RCs is $d(x^2 - y^2)$, as indicated in Fig. 6.

The Cu^{2+} hyperfine structure parameters give a measure of the distribution of the unpaired electron spin density (Abragam and Bleaney, 1970; Zeiger and Pratt, 1973). These quantities are difficult to evaluate because, in addition to their dependence on the spin-orbit interaction and the ligand field splittings, they depend on the radial ($\langle r^3 \rangle$) distribution of the electron density and on core polarization effects. The ratio $|A_\parallel / A_\perp|$ in other typical Cu compounds is $|A_\parallel / A_\perp| \approx 10$ for $d(x^2 - y^2)$ and $|A_\parallel / A_\perp| \approx 0.8$ for dz^2 orbital ground states (Abragam and Bleaney, 1970). When these values are compared with our experimental results we see again that the ground state for Cu^{2+} in RCs is a $d(x^2 - y^2)$ orbital.

The components of nitrogen hyperfine tensors $\vec{A}_{N_i}$ give a measure of the unpaired spin density at the ligand nuclei. They are an indication of the covalent bonding between the copper $d(x^2 - y^2)$ orbital and the ligand orbitals. This follows from the fact that the tails of the atomic orbital do not have a sizable density at the ligand nuclei, and the magnitude of the superhyperfine structure is measurable only because of its mixing with the ligand orbitals. The principal values of $\vec{A}_{N_i}$ obtained to first order for a strictly square planar arrangement of ligands around a copper ion having a ground state orbital $d(x^2 - y^2)$, are (Zeiger and Pratt, 1973):

$$A_N^3 = 2(N^2 A_{d-d} + \tfrac{1}{2} f_p A_p) + \tfrac{1}{2} f_s A_s, \qquad (7a)$$

$$A_N^1 = A_N^2 = -(N^2 A_{d-d} + \tfrac{1}{2} f_p A_p) + \tfrac{1}{2} f_s A_s, \qquad (7b)$$

where $f_s = \lambda_s^2 N^2$ and $f_p = \lambda_p^2 N^2$ represent, approximately, the fractions of time an electron spends in s and p ligand orbitals. N and λ_s, λ_p are the normalization constant and the covalent parameters, respectively, which enter in the definition of the molecular orbital. The remaining parameters in Eqs. 7 are given by:

$$A_p = \tfrac{4}{5} g_N \mu_N \mu_B \langle r^{-3} \rangle_p, \qquad (8a)$$

$$A_s = (16\pi/3) g_N \mu_N \mu_B |\Phi_s(0)|^2, \qquad (8b)$$

$$A_{d-d} = 2 g_N \mu_N \mu_B / a^3, \qquad (8c)$$

where g_N is the nuclear g factor and μ_N the nuclear magneton; $\langle r^{-3} \rangle_p$ is the mean value of r^{-3} over the p ligand orbital and $\Phi_s(0)$ is the value of the ligand wavefunction at the ligand nucleus. A_p and A_s of Eqs. 8a and b represent the contributions to the ligand hyperfine coupling constants of Eqs. 7a and b arising from p and s ligand atomic orbitals. A_{d-d} of Eq. 8c is the contribution arising from the averaged dipole–dipole interaction between the Cu^{2+} electron (in a d-orbital) and the ligand

nuclei, neglecting the spread of the Cu^{2+} wavefunctions. The distance between Cu^{2+} and the N ligand is a. As all quantities entering in Eqs. 8 are positive, it follows from Eqs. 7a and b that $|A_N^3| > |A_N^1|$, as observed experimentally (see Table 1). Similarly, the ratio $A_N^1(^{14}N)/A_N^1(^{15}N)$ of the hyperfine parameters for ^{14}N and ^{15}N is $g_N(^{14}N)/g_N(^{15}N) = 0.71$, as observed experimentally (see Table 1). The equality $A_N^1 = A_N^2$ used in the interpretation of the data is indicated by Eq. 7b.

In the highly symmetric complex shown in Fig. 6, a nitrogen ligand on the apical $\hat{z}$-axis (N_4) would not give rise to additional hyperfine structure since mixing between its s and p orbitals with the metal $d(x^2 - y^2)$ orbital is not allowed by symmetry. In the real, less symmetric case described by the crystallographic data of Allen et al. (1988) for $Fe^{2+}Q_A$:RCs, the square planar configuration of ligands is not exact. This allows mixing of the $d(x^2 - y^2)$ either directly with the s and p orbitals of N_4 or with the $d(z^2)$ orbital, which in turn can mix with the s and p orbitals. Either mechanism would produce an unpaired spin density at the apical ligand. However, the upper limit $|A_N| \leq 2.5 \times 10^{-4}$ cm^{-1} for the putative fourth ^{14}N nitrogen obtained from the linewidths of the hyperfine lines indicates that these admixtures are small.

ANALYSIS AND INTERPRETATION OF THE DATA ON $Cu^{2+}Q_A^-$:RCs

The spectrum displayed in Fig. 4, obtained from a chemically reduced $Cu^{2+}Q_A^-$:RCs sample is not a simple superposition of the Cu^{2+} spectrum of Fig. 1 with the narrow signal of the reduced quinone observed at $g_Q = 2.0046$ in samples where the metal ion was removed (Feher et al., 1972). The reason is that we are dealing with a magnetic $Cu^{2+}Q_A^-$ spin dimer, in which the spins of Cu^{2+} and Q_A^- are coupled by exchange and by dipole–dipole interactions.

The EPR spectrum of a magnetic dimer has been analyzed by several authors (see e.g., Kokoszka and Gordon, 1969; Abragam and Bleaney, 1970). We present first an elementary model containing the basic physical ingredients to gain a qualitative understanding of the EPR spectrum of the dimer. Then, we examine a more detailed model which was used to analyze the experimental data and to evaluate the parameters of the interaction.

Isotropic model

In the elementary model, the Hamiltonian describing the spins $\vec{S}_{Cu}$ and $\vec{S}_{Q_2}$ having isotropic g factors $g_{Cu} \neq g_Q$, in a magnetic field $\vec{H}$, and interacting through an isotropic

exchange coupling of magnitude J_0, is written as:

$$H = g_{Cu}\mu_B H S_{Cu}^z + g_Q\mu_B H S_Q^z - J_0 \vec{S}_{Cu} \cdot \vec{S}_Q, \qquad (9)$$

where $S_{Cu} = S_Q = \frac{1}{2}$. This spin dimer has four energy levels which were calculated in the basis set $|S_{Cu}^z, S_Q^z\rangle$ by diagonalyzing the 4×4 Hamiltonian matrix.

$$E_1 = g\mu_B H - J_0/4, \qquad (10a)$$

$$E_2 = J_0/4 + \sqrt{J_0^2/4 + (G\mu_B H)^2}, \qquad (10b)$$

$$E_3 = J_0/4 - \sqrt{J_0^2/4 + (G\mu_B H)^2}, \qquad (10c)$$

$$E_4 = -g\mu_B H - J_0/4, \qquad (10d)$$

where $g = \frac{1}{2}(g_{Cu} + g_Q)$ and $G = \frac{1}{2}(g_{Cu} - g_Q)\mu_B H$.

In the absence of a magnetic field Eqs. 10 reduce to:

$$E_1 = E_3 = E_4 = -J_0/4 \quad \text{and} \quad E_2 = 3J_0/4.$$

If $J_0 > 0$, the lowest energy state is a spin triplet, with the singlet excited state separated by an energy J_0, from the ferromagnetic ground state. If $J_0 < 0$ the arrangement of the spins is anti-ferromagnetic, with the ground state being a spin singlet.

A microwave field induces transitions between the energy levels of Eqs. 10 as depicted in Fig. 7 *a*. The allowed transitions are $1 \leftrightarrow 2$, $1 \leftrightarrow 3$, $2 \leftrightarrow 4$, and $3 \leftrightarrow 4$. If $J_0 = 0$, Eqs. 10 predict two resonances at fields $H_{Cu} = h\nu/(g_{Cu}\mu_B)$ and $H_Q = h\nu/(g_Q\mu_B)$, corresponding to noninteracting copper and quinone spins. These transitions are indicated by solid arrows in Fig. 7 *a*, and the resulting spectrum is shown as a stick diagram in Fig. 7 *b*. For $J_0 \neq 0$, but $|J_0| \ll \frac{1}{2}|g_{Cu} - g_Q|\mu_B H$ (see Eqs. 10), one observes four resonances at $H_{Cu} \pm \frac{1}{2} J_0/(g_{Cu}\mu_B)$ and $H_Q \pm \frac{1}{2} J_0/(g_Q\mu_B)$ as shown by the dashed lines and arrows in Fig. 7 *a* and by the stick diagram in Fig. 7 *c*. As $|J_0|$ increases, the resonances $1 \leftrightarrow 2$ and $2 \leftrightarrow 4$ move out, losing intensity and the resonances $1 \leftrightarrow 3$ and $3 \leftrightarrow 4$ move toward the center of the spectrum. For $|J_0| \gg \frac{1}{2}|g_{Cu} - g_Q|\mu_B H$ they collapse into a single line at $H_0 = \frac{1}{2}(H_{Cu} + H_Q) = h\nu/(g\mu_B)$, as shown in Fig. 7 *d*.

The situation is conceptually similar when one of the spins ($\vec{S}_{Cu}$) has also a hyperfine coupling with the nuclear spin $\vec{I}_{Cu}$. The spectra of the exchange coupled $Cu^{2+}Q_A^-$ spin dimer, with $\vec{S}_{Cu}$ coupled to $\vec{I}_{Cu}$ ($^{65}I = \frac{3}{2}$) via hyperfine interaction is sketched in Figs. 7 *e* and *f*, for the limiting cases $J_0 = 0$ and $|J_0| \gg |g_{Cu} - g_Q|\mu_B H/2$. For $J_0 = 0$ (Fig. 7 *e*) one observes the superposition of the spectrum of $\vec{S}_{Cu}$ with the expected four hyperfine lines and the single line spectrum due to $\vec{S}_Q$. For $|J_0| \gg |g_{Cu} - g_Q|\mu_B H/2$, one observes in Fig. 7 *f* an averaging similar to that displayed in Fig. 7 *d*. However, in this case the position of each resonance of the low field hyperfine quartet of copper is "averaged" with the position of the
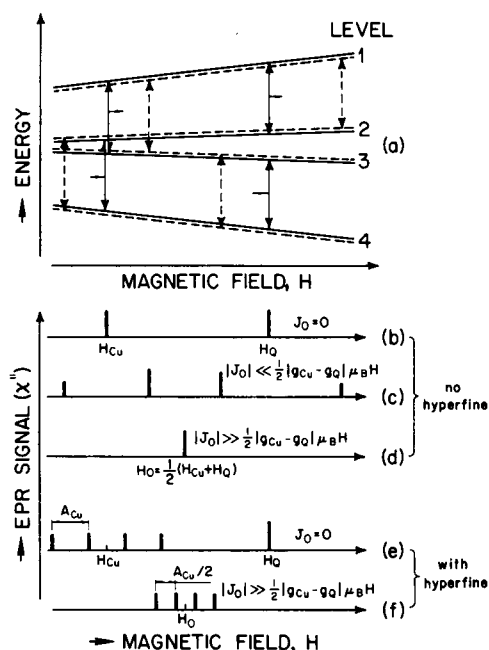

FIGURE 7 Energy levels and EPR transitions of the elementary model (isotropic g values) of the spin dimer $Cu^{2+}Q_A^-$:RC. (*a*) Energy level scheme calculated with Eqs. 10 for $J_0 = 0$ (*solid lines*) and a small $J_0 > 0$ (*dashed lines*). The positions of the allowed transitions are indicated by solid (for $J_0 = 0$) and dashed arrows (for $|J_0| > 0$). (*b*) Stick diagram of the EPR spectrum for $J_0 = 0$. Two resonance lines corresponding to the two isolated paramagnetic centers are predicted. (*c*) EPR spectrum for a small positive J_0. (*d*) EPR spectrum for large J_0. (*e*) EPR spectrum for $J_0 = 0$, including the hyperfine interaction with the copper nucleus ($I_{Cu} = \frac{3}{2}$). (*f*) Same as *e* but for large J_0.

quinone resonance, giving a single hyperfine quartet around H_0, with the splitting having half the value of that for $J_0 = 0$. The situation that is intermediate between the limiting cases shown in Figs. 7 *e* and *f* (i.e., the one corresponding to Fig. 7 *c*) is the most interesting one, because it allows one to determine $|J_0|$. Note that the description of the EPR spectrum of a spin dimer shown in Fig. 7 is independent of the sign of J_0.

The previous discussion provides a qualitative understanding of the spectrum for $Cu^{2+}Q_A^-$:RCs shown in Figs. 4 and 5 *a*. The value of J_0 can be determined from the positions and splittings of the resonance peaks. However, in the simple model described above, we assumed an isotropic interaction between $\vec{S}_{Cu}$ and $\vec{S}_Q$, (Heisenberg type). To provide a quantitative explanation of the data we need to consider a more elaborate model involving an anisotropic magnetic interaction. The EPR spectra of dimers in which one or both ions have hyperfine structures have been discussed by several authors for the limiting case of an exchange interaction that is much larger than the difference between the Zeeman energies for the two spins (see, e.g., Kokoszka and Gordon, 1969). This case,

shown in Fig. 7 f, does not apply to our problem. We present below a model which is more appropriate to our system.

Anisotropic model

The spin Hamiltonian for the copper-quinone system can be written as

$$H = H_{Cu} + H_Q + H_{int},$$

where H_{Cu}, H_Q, and H_{int} represent the spin Hamiltonian of the Cu^{2+} ion, the quinone, and the interaction between the Cu^{2+} and quinone spins, respectively. H_{Cu} for the spin $\vec{S}_{Cu}$ of the copper ion is given by Eq. 1, where the anisotropic g tensor and hyperfine tensor are represented by $\vec{g}_{Cu}$ and $\vec{A}_{Cu}$. The small ligand hyperfine coupling will not be considered for simplicity in the analysis of the spectrum of $Cu^{2+}Q_A^-$:RCs. The spin $\vec{S}_Q$ of the reduced quinone is approximately isotropic and does not exhibit a resolvable hyperfine interaction. Its spin Hamiltonian is given by:

$$H_Q = g_Q \mu_B \vec{H} \cdot \vec{S}_Q. \quad (11)$$

The Hamiltonian describing the interaction between $\vec{S}_{Cu}$ and $\vec{S}_Q$ is given by:

$$H_{int} = -J_0 \vec{S}_{Cu} \cdot \vec{S}_Q + \vec{S}_{Cu} \cdot \vec{D} \cdot \vec{S}_Q, \quad (12)$$

where the first term is the Heisenberg exchange introduced in Eq. 9 and the second term represents an anisotropic magnetic interaction with $\vec{D}$ assumed to be a traceless and symmetric tensor. The anisotropic term may arise from dipole–dipole interaction or from mechanisms involving exchange interactions and spin-orbit coupling (Moriya, 1960; Kanamori, 1963). Defining:

$$\vec{S} = \vec{S}_{Cu} + \vec{S}_Q, \quad \vec{\sigma} = \vec{S}_{Cu} - \vec{S}_Q,$$

$$\vec{g} = \frac{1}{2}(\vec{g}_{Cu} + \vec{g}_Q) \quad \text{and} \quad \vec{G} = \frac{1}{2}(\vec{g}_{Cu} - \vec{g}_Q),$$

with $\vec{g}_Q = g_Q \vec{U}$ (where $\vec{U}$ is a unit tensor), the Hamiltonian $H_{Cu} + H_Q$ (Eqs. 1 and 11) can be written as:

$$H_{Cu} + H_Q = \mu_B \vec{S} \cdot \vec{g} \cdot \vec{H} + \frac{1}{2} \vec{I}_{Cu} \cdot \vec{A}_{Cu} \cdot \vec{S}$$
$$+ \mu_B \vec{\sigma} \cdot \vec{G} \cdot \vec{H} + \frac{1}{2} \vec{I}_{Cu} \cdot \vec{A}_{Cu} \cdot \vec{\sigma}. \quad (13)$$

Because $\vec{D}$ is symmetric, Eq. 12 can be rewritten as:

$$H_{int} = -\frac{1}{2} J_0(S^2 - \frac{3}{2}) + \frac{1}{4} \vec{S} \cdot \vec{D} \cdot \vec{S} - \frac{1}{4} \vec{\sigma} \cdot \vec{D} \cdot \vec{\sigma}. \quad (14)$$

We assume that $H = H_{Cu} + H_Q + H_{int}$ can be separated

into $H_0 + H'$, where H_0 is given by:

$$H_0 = \mu_B \vec{S} \cdot \vec{g} \cdot \vec{H} - \frac{1}{2} J_0(S^2 - \frac{3}{2}), \quad (15)$$

and H' contains the remaining terms as a perturbation. Only the secular contributions to H' will be retained, neglecting the nondiagonal terms in the base where H_0 of Eq. 15 is diagonal. This simplification is appropriate to explain the EPR data in powders; without it the problem is more complicated and requires the diagonalization of a 16×16 matrix.

To solve the problem we choose $\hat{\zeta} = \vec{g} \cdot \hat{h}/g$ and $\hat{\zeta}' = \vec{A}_{Cu} \cdot \vec{g} \cdot \hat{h}/|\vec{A}_{Cu} \cdot \vec{g} \cdot \hat{h}|$ respectively as the quantization axes for $\vec{S}$ and $\vec{\sigma}$, and for the nuclear spin $\vec{I}_{Cu}$. In this system of axes we obtain:

$$H = H_0 + H' = g\mu_B H S_{\zeta} - \frac{1}{2} J (S^2 - \frac{3}{2}) + \frac{1}{2} \alpha I_{Cu}^{\zeta'} S_{\zeta}$$
$$+ \frac{1}{2} \alpha I_{Cu}^{\zeta'} \sigma_{\zeta} + F\mu_B H \sigma_{\zeta} + \frac{1}{2} d(S_{\zeta}^2 - \frac{1}{2}) \quad (16)$$

with

$$g^2 = \hat{h} \cdot \vec{g} \cdot \vec{g} \cdot \hat{h} \quad \text{and} \quad g^2 \alpha^2 = \hat{h} \cdot \vec{g} \cdot \vec{A}_{Cu} \cdot \vec{A}_{Cu} \cdot \vec{g} \cdot \hat{h},$$

where $J = J_0 + d/3$ and $F = \hat{h} \cdot \vec{g} \cdot \vec{G} \cdot \hat{h}/g$. The anisotropy parameter,

$$d = 3(\hat{h} \cdot \vec{g} \cdot \vec{D} \cdot \vec{g} \cdot \hat{h})/2(\hat{h} \cdot \vec{g} \cdot \vec{g} \cdot \hat{h})$$

in Eq. 16 is the projection of the $\vec{D}$ tensor along the direction $\hat{\zeta} = \vec{g} \cdot \hat{h}/g$. In our calculations we assume that $|J_0| \gg |d|$ (as confirmed by the experimental results). Then $J \approx J_0$ gives the magnitude of an effective Heisenberg exchange. The Hamiltonian of Eq. 16 predicts an EPR spectrum of 16 lines whose positions are given by:

$$H_{1,m} = H_0 + \frac{1}{2} J_0/(g\mu_B) - \frac{1}{2} d/(g\mu_B)$$
$$- \frac{1}{2} \alpha m/(g\mu_B) + \Omega(m), \quad (17a)$$

$$H_{2,m} = H_0 + \frac{1}{2} J_0/(g\mu_B) - \frac{1}{2} d/(g\mu_B)$$
$$- \frac{1}{2} \alpha m/(g\mu_B) - \Omega(m), \quad (17b)$$

$$H_{3,m} = H_0 - \frac{1}{2} J_0/(g\mu_B) + \frac{1}{2} d/(g\mu_B)$$
$$- \frac{1}{2} \alpha m/(g\mu_B) - \Omega(m), \quad (17c)$$

$$H_{4,m} = H_0 - \frac{1}{2} J_0/(g\mu_B) + \frac{1}{2} d/(g\mu_B)$$
$$- \frac{1}{2} \alpha m/(g\mu_B) + \Omega(m), \quad (17d)$$

where $m = m_{Cu} = (\frac{3}{2}, \frac{1}{2}, -\frac{1}{2}, -\frac{3}{2})$ are the possible projections of I_{Cu}^{ζ} on the z-axis. We define $\Omega(m) = [J_0^2/4 + R^2(m)]^{1/2}/(g\mu_B)$, with $R(m) = F\mu_B H + \alpha m/2$.

The central field H_0 is related to the microwave frequency ν by $H_0 = h\nu/(g\mu_B)$.

On replacing J_0 by $-J_0$ and d by $-d$ it is seen that Eqs. 17a and b exchange their roles with Eqs. 17d and c, respectively. Thus, the EPR spectrum depends only on the relative signs of J_0 and d; consequently their absolute signs cannot be determined from the EPR data. Other experimental techniques, (e.g., magnetic susceptibility) could provide the sign of J_0, and then the sign of d can be determined from the EPR spectra. We shall assume $J_0 < 0$, the same sign as determined for $Fe^{2+}Q_A^-$:RCs (Butler et al., 1984).

Eqs. 17a–d predict hyperfine splittings $|H_{i,m} - H_{i,m-1}|$ of the four groups, i, of lines that depend on J_0 and m, but not on d, whereas the effective g factor corresponding to the field of the center of the quartet:

$$H_i = \frac{1}{4} \sum_m H_{i,m}$$

depends on both, J_0 and d. These considerations allow us to use Eqs. 17 to calculate J_0 and d from the experimental data.

The spectrum as a function of the isotropic exchange J_0: determination of J_0

The positions of the EPR lines predicted by Eqs. 17a–d are shown in Fig. 8 as a function of J_0 in the absence of anisotropic interaction ($d = 0$). The calculations were
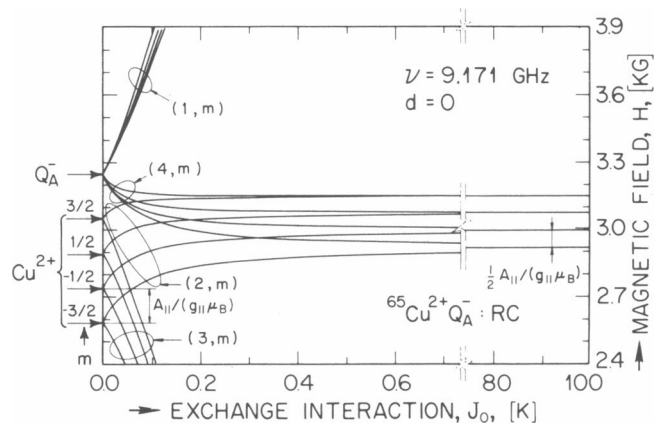
FIGURE 8 Values of the magnetic field at which resonances are predicted by Eqs. 17a–d as a function of J_0, for $d = 0$. At $J_0 = 0$, two sets of lines corresponding to the isolated Q_A^- and Cu^{2+} ions are obtained. For $J_0 \neq 0$, there are sixteen lines. The horizontal axis is broken and its scale changed to show the asymptotic behavior for large J_0; for this case a single group of four lines, with a hyperfine splitting equal to half of that obtained for the copper resonance at $J_0 = 0$, is observed ($m = m_{Cu}$).

performed for the applied field $\vec{H}$ along the parallel direction. The following values were used, $g_{Cu} = g_\parallel = 2.314$, $A_{Cu} = A_\parallel = -167 \times 10^{-4}$ cm^{-1}, $g_Q = 2.0046$ (Feher et al., 1972), $\nu = 9.171$ GHz, (see Figs. 4 and 5), $g = \frac{1}{2}(g_\parallel + g_Q) = 2.159$ and $F = \hat{h} \cdot \vec{g} \cdot \vec{G} \cdot \vec{g} \cdot \hat{h}/g \approx \frac{1}{2}(g_\parallel - g_Q) = 0.154$. The asymptotic result obtained for large $|J_0|$ is indicated on the right of Fig. 8.

For $J_0 = 0$, $\vec{S}_{Cu}$ and $\vec{S}_Q$ are uncoupled. There is a single resonance corresponding to $\vec{S}_Q$, at field $H_{1,m} = H_{4,m}$, and four resonances corresponding to the Cu^{2+} ion, at fields $H_{2,m} = H_{3,m}$, whose positions depend on the nuclear spin quantum number m. As J_0 increases, there are 16 transitions. Each of the four Cu^{2+} hyperfine lines split into two components. This doubling is due to the difference in the effective magnetic fields at a copper site, when its quinone partner has its spin up or down ($S_Q^z = \pm\frac{1}{2}$). The hyperfine splittings within these two groups of resonances decrease with increasing J_0. The quinone resonance in Fig. 8 splits into two groups of four lines. The group described by $H_{4,m}$ moves down in field, whereas the group $H_{1,m}$ moves up in field, both with increasing hyperfine splittings. Each group of resonances is related to one of the spin states of copper. The spin $\vec{S}_Q$ also interacts indirectly with the nuclear spin of copper $\vec{I}_{Cu}$ through the exchange interaction between $\vec{S}_{Cu}$ and $\vec{S}_Q$, giving rise to the four line hyperfine pattern. As in the case with no hyperfine structure, analyzed by Abragam and Bleaney (1970), the groups of resonances $(1, m)$ and $(3, m)$ diverge from the central field position (Eqs. 17a and c); their intensity decreases with increasing J_0, as can be proven by calculating the wavefunctions and transition probabilities. The groups $(2, m)$ and $(4, m)$ (Eqs. 17b and d) tend to merge around H_0. For $J_0 \to \infty$ and $d = 0$, they collapse into a single group with four hyperfine components; the observed splitting is half of that for the uncoupled Cu^{2+} ion. This asymptotic result has been discussed by several authors (Kokoszka and Gordon, 1969; Abragam and Bleaney, 1970), and is sketched in Fig. 7 f. For intermediate values of J_0, Fig. 8 shows a complex crossing of the eight nondivergent lines.

The EPR spectrum of $Cu^{2+}Q_A^-$:RC displayed in Fig. 4 and blown up in Fig. 5 a, shows a complex structure with several peaks. To emphasize the peaks, a baseline generated by a polynomial was subtracted from the spectrum; the result is displayed in Fig. 5 b. There are four peaks separated by ~100 G, which are tentatively labeled as $H_{2,m}$, with $m = -\frac{3}{2}, -\frac{1}{2}, \frac{1}{2}, \frac{3}{2}$, and having a g value $g = 2.21$. There is a fifth peak between the third and the fourth lines of the first group, which we assume to belong to group 4.

As pointed out before, the hyperfine splitting of the different groups of lines do not depend on the anisotropy parameter d, but only on J_0. In Fig. 9, we plot $\delta H_{hyp}(2) = |H_{2,-3/2} - H_{2,-1/2}|$ and $\delta H_{hyp}(4) = |H_{4,-3/2} - H_{4,-1/2}|$ as
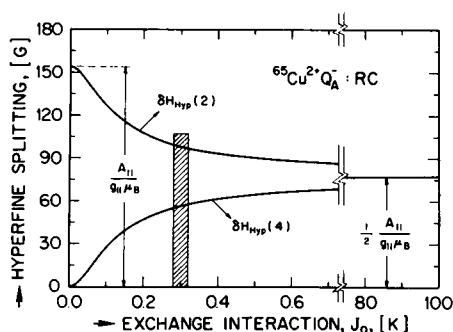
FIGURE 9 Hyperfine splittings $\delta H_{Hyp}(2) = |H_{2,-3/2} - H_{2,-1/2}|$ and $H_{Hyp}(4) = |H_{4,-3/2} - H_{4,-1/2}|$ of Cu^{2+} as a function of J_0. These splittings represent the two lower field hyperfine components of the groups of resonances (2, m) and (4, m) shown in Fig. 5. They were calculated from Eqs. 17b and d, and are independent of the anisotropy parameter d. The cross-hatched area indicates the value of J_0 obtained by comparing the experimental value of δ_{Hyp} (2) (Fig. 5) with the calculated ones. The horizontal axis is broken and its scale changed to show the asymptotic behavior for large J_0; in this case $\delta H_{Hyp}(2) = \delta H_{Hyp(4)} = A_{\|}/(g_{Cu}\mu_B)$ i.e., half of the hyperfine splitting of copper for $J_0 = 0$.

a function of J_0 in the parallel direction, as obtained from Eqs. 17b and d. Eqs. 17a and d also show that $\delta H_{hyp}(2) + \delta H_{hyp}(4) = A_{\|}/(g\mu_B)$, independent of J_0. For $J_0 \rightarrow \infty$, both $\delta H_{hyp}(2)$ and $\delta H_{hyp}(4)$ are equal to $\frac{1}{2} A_{\|}/(g\mu_B)$, as expected. The observed 98.7 G splitting between the $H_{2,-3/2}$ and $H_{2,-1/2}$ peaks (see Fig. 5 b) corresponds to $|J_0| = 0.30$ K (see cross-hatched area in Fig. 9). This value is taken as the isotropic exchange parameter Eq. 12 to be used in the identification of the other EPR lines.

The effect of the anisotropic component (d) on the spectrum: determination of d

In Fig. 8 we neglected the anisotropic exchange interaction introduced in Eq. 12. To evaluate the magnitude of the anisotropic part of the interaction, the positions of the resonance lines of the two central groups $H_{2,m}$ and $H_{4,m}$ obtained from Eqs. 17 are plotted in Fig. 5 c as a function of d, for -0.03 K $< d < 0.03$ K, and $J_0 = 0.30$ K. The effect of the anisotropy is to move these groups out of the $g \approx 2$ region, in opposite directions; in one direction for $d > 0$, and in the other for $d < 0$ (see Fig. 5 c). By matching the predicted positions of the lines (Fig. 5 c) with the observed lines (Fig. 5 b), the value $d = 0.010$ K is obtained (see horizontal arrow in Fig. 5 c). It is seen from a simple analysis that the fourth peak going from low to high fields is assigned to group 4. The resonances $H_{2,1/2}$ and $H_{4,-3/2}$ are superimposed, as are those $H_{2,3/2}$

and $H_{4,1/2}$. We conclude that the values

$$J_0 = (-0.30 \pm 0.03) \text{ K} \quad \text{and} \quad d = (-0.010 \pm 0.002) \text{ K}$$

represent the best fit to the observed spectrum. As discussed before, the predicted EPR spectrum does not change when the signs of J_0 and d are changed together. The signs given above were chosen in analogy with the sign of J_0 determined for the $Fe^{2+}Q_A^-$ spin dimer (Butler et al., 1980, 1984).

A complete simulation of the spectrum of the reduced sample was not attempted. The reason is the large number of parameters (because $\vec{D}$ is a traceless tensor, there are five additional parameters), which makes a meaningful simulation questionable. Consequently, data obtained in randomly oriented molecules allow one to determine only the Heisenberg (isotropic) component of the exchange interaction, and the projection d of the $\vec{D}$ tensor along the normal to the $d(x^2 - y^2)$ ground state orbital of the Cu^{2+} ion.

SUMMARY AND DISCUSSION

We have investigated the electronic structure of Cu^{2+} in reaction centers of *Rb. sphaeroides* by EPR spectroscopy. The values of the hyperfine interaction of the unpaired electron on Cu^{2+} with the ^{65}Cu nucleus, the superhyperfine interaction with the nearby nitrogen ligands and the magnetic interaction between Cu^{2+} and Q_A^- were obtained and compared with a model based on the recently determined three-dimensional structure (Allen et al., 1987, 1988).

The copper hyperfine interaction and g tensor in unreduced $Cu^{2+}Q_A$:RCs

The EPR spectrum of unreduced $Cu^{2+}Q_A^-$:RCs was analyzed by assuming that the g tensor and copper hyperfine tensor have the same principal axes (see Table 1). This hypothesis has been verified in simpler model systems (Schweiger et al., 1982), and is believed to hold for macromolecules as well (Solomon et al., 1983). This hypothesis is also supported by the sharpness of the low field peaks of the EPR spectra shown in Figs. 2 and 3.

The values obtained for $g_\|$, $g_\perp$, $A_\|$, and $A_\perp$ clearly show that the ground state orbital of the unpaired electron of Cu^{2+} is $d(x^2 - y^2)$ (see e.g., Zeiger and Pratt, 1973; Solomon et al., 1983). This is the expected ground state for an octahedral environment of Cu^{2+} as shown for the simplified model in Fig. 6. To check whether the octahedral symmetry is compatible with the recently determined

structure of the RC from *Rb. sphaeroides* (Allen et al., 1987, 1988), we assume that the Cu^{2+}:RC structure is isomorphous with the native Fe^{2+}:RC structure.[4] Fig. 10 shows the structure around the metal ion using the crystallographic data of Allen et al. (1987, 1988). One can easily discern a distorted octahedron with its base plane (shaded area) formed by ligands to N_1, N_2, N_3, O_6 and with N_4, O_5 at the apex. The lobes of the $d(x^2 - y^2)$ wavefunction in the base plane are also indicated. An alternate orientation of the $d(x^2 - y^2)$ orbital with the base plane formed by N_1, N_3, N_4, and O_5 would produce a more distorted octahedron and is considered less likely, although it was favored by Evelo et al. (1988) in their analysis of the limited angular variation of EPR spectra in single crystals of RCs from *Rps. viridis*. A more complete investigation of EPR spectra in single crystals should provide a definitive determination of the orientation of the orbitals with respect to the molecular structure.

The ^{14}N and ^{15}N superhyperfine interaction in unreduced $Cu^{2+}Q_A$:RCs

The unpaired electron on Cu^{2+} interacts also with the nuclei of the nitrogen ligands. In the parallel direction this superhyperfine interaction is about an order of magnitude smaller than the hyperfine interaction with the ^{65}Cu nucleus (see Table 1). From the number of lines of the EPR spectrum (see Figs. 2 and 3) we determined that Cu^{2+} interacts only with three of the four possible nitrogens associated with the four histidines L190, L230, M229, and M268 (Fig. 10). This result can be interpreted by considering the model shown in Figs. 6 and 10. The $d(x^2 - y^2)$ orbital of Cu^{2+} has a high electron density at the nitrogens N_1, N_2, and N_3, but only a small density at the apical position of N_4. Consequently, the superhyperfine interaction with N_4 is too small to be resolved in our EPR experiments. A similar situation has been observed in the Cu^{2+} complex of superoxide dismutase, which displays superhyperfine splitting from 3 nitrogens from coordinated histidines, although the x-ray structure shows Cu^{2+} to be coordinated to 4 histidine nitrogens (Van Camp et al., 1982). The small hyperfine interaction from the fourth nitrogen might be resolved by other techniques,

---

[4]The validity of this assumption is supported by the observation that the electron transfer rate from Q_A^- to Q_B is the same in Cu^{2+}:RCs and Fe^{2+}:RCs. (Debus et al., 1986). Small changes in the position of the ligands cannot, however, be excluded (Cotton and Wilkinson, 1980). It has been found in other systems that when a metal ion (Zn^{2+}) is replaced by Cu^{2+} a change in ligand geometry occurs, which results in a more symmetric octahedral environment around the Cu^{2+} (Steren et al., 1989).
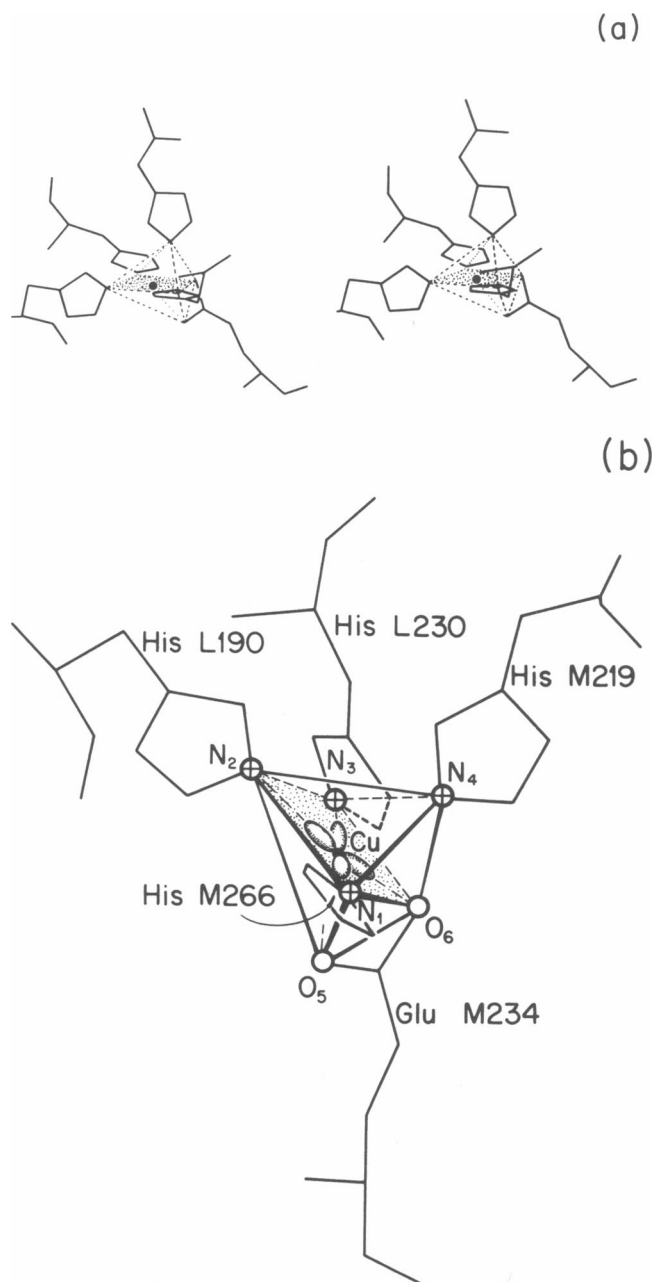

FIGURE 10 Structure of the photosynthetic reaction center from *Rb. sphaeroides* around the metal ion, as obtained from the crystallographic data of Allen et al. (1988). (*a*) Stereoview of the structure of Cu^{2+} (*circle*) with its nearest ligands and amino acid residues. (*b*) Monoview of the structure shown in *a*, enlarged and slightly rotated. Note the approximate octahedral environment of Cu^{2+}. The base plane of the octahedron formed by N_1, N_2, N_3, O_6 is shaded. The position proposed for the $d(x^2 - y^2)$ ground state orbital is sketched. Compare with the simplified model of Fig. 6.

e.g., electron spin-echo envelope modulation (Mims and Peisach, 1989).

Buchanan and Dismukes (1987) reported nitrogen superhyperfine interactions in RCs from a different strain of *Rb. sphaeroides* (wild type, strain Y) in which the Cu^{2+} was biosynthetically incorporated. Their EPR spectra are very different from ours and show an interaction with four nitrogens. How can we reconcile the discrepancy between our results? One possibility is that the Cu^{2+} is incorporated into a site different from the Fe binding site (e.g., a nonspecific site) in one of the two preparations. Evidence against this include the stoichiometry for Cu in both preparations, i.e., the observation that the sum of the stoichiometry for Cu plus Fe is close to 1 metal/RC. Additional support for the binding of the Cu to the Fe binding site is the observation of the $Cu^{2+}Q^-$ EPR signal upon quinone reduction as shown in our sample. Buchanan and Dismukes also report that changes in the EPR spectrum of Cu in their sample were observed upon quinone reduction, although no spectra were shown. A second possibility is that there may be differences between the Cu^{2+} binding sites due to differences between chemical reconstitution (which we used) and biosynthetic incorporation. Evidence that the chemically reconstituted RCs retain their native structure is provided by the finding that RCs chemically reconstituted with Cu have essentially the same electron transfer rates as native RCs (Debus et al., 1986). A third possibility is that RCs from the bacterial strains used by the two groups are different. So far we were not successful in biosynthetically incorporating significant amounts of Cu^{2+} in the R-26 strain.

The isotropic exchange interaction J_0 between Cu^{2+} and Q_A^-

The magnitude of the isotropic exchange interaction between Cu^{2+} and Q_A^- in reduced RCs was obtained from the Hamiltonian of Eq. 16, keeping only nonsecular terms in the base in which H_0 is diagonal. This allowed us to obtain Eqs. 17 by diagonalizing a 4 × 4 matrix, instead of the 16 × 16 matrix corresponding to the whole coupled spin system, thereby neglecting the admixtures of eigenvectors corresponding to different nuclear spin quantum numbers of copper. This approximation introduced an uncertainty of a few percent in the value calculated for the hyperfine splitting and the isotropic and anisotropic magnetic interactions J_0 and d. The uncertainty associated with experiments performed on powder samples does not justify a more elaborate theoretical treatment.

The value of $|J_0|$ obtained for Cu^{2+} is 0.30 K, which is close to the value $J_0 = -0.43$ K obtained by Butler et al. (1984) for Fe^{2+} in native RCs. In that case the interaction was determined to be antiferromagnetic, which by analogy led us to assume a negative sign for J_0 in $Cu^{2+}Q_A^-$: RCs. The similarity in the value of J_0 for $Cu^{2+}Q_A^-$ and $Fe^{2+}Q_A^-$ suggests that the magnitude of the superexchange interaction depends only weakly on the metal involved but is expected to depend more strongly on the nature of the chemical paths connecting the unpaired spins.

The value of J_0 obtained from our data for the $Cu^{2+}Q_A^-$:RCs may be compared with those considered by Coffman and Buettner (1979). Their limit function predicts a metal-quinone distance shorter than 10 Å, which is not far from the crystallographic value (11 Å) obtained by Allen et al. (1987) between the metal ion and the center of Q_A. Thus, the magnitude of the superexchange interaction between Cu^{2+} and Q_A^- is well within expectations.

Exchange interactions (J_0) between species separated by long distances bridged by one or more nonmagnetic atoms (superexchange interaction), have been described by Anderson (1959) and Hay et al. (1975). Although the general problem is well understood, specific calculations are complicated even for systems much simpler than ours. Consequently, we shall discuss superexchange between Cu^{2+} and Q_A^- only in qualitative terms.

Superexchange paths may be divided into sections, each involving a nonmagnetic ion or a simple molecule. Sections containing strong overlap of orbitals or covalently bonded groups provide efficient pathways for superexchange. The path of the $Cu^{2+}Q_A^-$ system can be divided into three sections (see Fig. 11). The first is
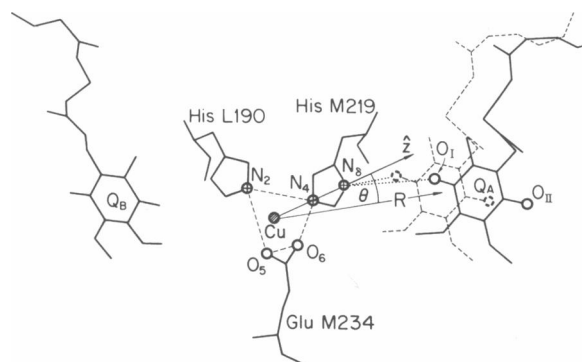

FIGURE 11 Structure of the photosynthetic reaction center from *Rb. sphaeroides* around the metal ion, obtained from the crystallographic data of Allen et al. (1988). The figure includes nearby amino acid residues and the quinone acceptors Q_A and Q_B; the carbonyl oxygens of Q_A are also indicated. From the distance R and angle θ, defined in the text, the magnitude of the dipole–dipole interaction between the Cu^{2+} ion and Q_A^- was evaluated. Dashed lines show the position of the quinone obtained upon reduction, as suggested by Allen et al. (1988) and supported by our results.

between Cu^{2+} and N_4 of the imidazole ring of His M219, the second is the imidazole ring, and the third connects the N_δ nitrogen of the imidazole with the oxygen O_I of Q_A (dotted line, Fig. 11).

The first section connects Cu^{2+} with the apical ligand N_4 (Figs. 10 and 11). The unpaired electron density of the $d(x^2 - y^2)$ ground state orbital of Cu^{2+} is small at the position of N_4. Consequently, in spite of the short path connecting Cu^{2+} and N_4, this section produces a strong restriction on the magnitude of the superexchange coupling. This has been shown for simple Cu^{2+}-amino acid model systems, in which the exchange interaction between Cu^{2+} ions has been evaluated as a function of the distance between Cu^{2+} and the apical ligand (Levstein and Calvo, 1990).

The second section of the superexchange path is the imidazole ring; it is made of covalently bonded atoms with a stable geometry. This section will not significantly restrict the superexchange coupling, nor is its geometry expected to change upon reduction of Q_A or replacement of Fe^{2+} by Cu^{2+}.

The third section connecting N_δ of the imidazole with O_I of Q_A^- may put another strong restriction on the magnitude of the superexchange interaction since the overlap of the electron densities between these two atoms is small. The distance between N_δ and O_I, determined by x-ray diffraction, is too large (4.5 Å) to form a hydrogen bond (Allen et al., 1988). However, it should be kept in mind that the x-ray data were obtained on RCs with an unreduced quinone. When Q_A is reduced, the quinone ring could be displaced to an alternate, sterically unhindered, position as has been suggested by Allen et al. (1988) (dashed line, Fig. 11). In this position a hydrogen bond could be formed between N_δ and O_I, which would greatly enhance the exchange coupling.

Dipole–dipole interaction between Cu^{2+} and Q_A^- in reduced $Cu^{2+}Q_A^-$:RCs

To explain the data in $Cu^{2+}Q_A^-$:RCs we introduced an anisotropic (tensorial) magnetic interaction between $\vec{S}_{Cu}$ and $\vec{S}_Q$ (Eq. 12). The tensor $\vec{D}$ is assumed to be symmetric; antisymmetric interactions do not contribute to the EPR spectra.

Different microscopic mechanisms may contribute to $\vec{D}$, whose projection $d = -0.010$ K along the parallel axis was evaluated. They have been analyzed by Moriya (1960) and Kanamori (1963), whose results indicate that the contribution to d arising from the exchange interaction is smaller than the experimentally observed value, and, as a first approximation can be neglected in our

analysis.[5] Therefore, the value $d = -0.010$ K reported here for $Cu^{2+}Q_A^-$:RCs is attributed to the dipole–dipole interaction between Cu^{2+} and Q_A^-.

Because the Zeeman terms of Eq. 13 are larger than the dipole–dipole interaction, we consider only the secular part H_{dd}, given by

$$H_{dd} = [(g_{Cu}g_Q\mu_B^2/(2\langle R^3\rangle)]$$
$$\cdot (3S_{Cu}^h S_Q^h - \vec{S}_{Cu} \cdot \vec{S}_Q)(1 - 3\cos^2\theta), \quad (18)$$

where R is the distance between a point dipole at the Cu^{2+} site and the unpaired spin distribution of Q_A^- and $\langle R^3\rangle$ is the mean value of R^3 over this distribution. The angle θ is measured between the direction $\hat{h}$ of the applied magnetic field (the parallel direction in our experiments) and the $Cu^{2+} - Q_A^-$ axis. These distances and directions are indicated in Fig. 11. Eq. 18 can be written in terms of the total spin $\vec{S} = \vec{S}_{Cu} + \vec{S}_Q$ to give:

$$H_{dd} = [(g_{Cu}g_Q\mu_B^2/(4\langle R^3\rangle)]$$
$$\cdot [3(S^h)^2 - S(S + 1)](1 - 3\cos^2\theta). \quad (19)$$

Comparing Eqs. 16 and 19 we find:

$$d = [(3\, g_{Cu}g_Q\mu_B^2/(2\langle R^3\rangle)](1 - 3\cos^2\theta). \quad (20)$$

A value $\langle R^3\rangle^{1/3} = 10$ Å is obtained from the structural data of Allen et al. (1987, 1988) assuming that the unpaired spin of Q_A^- is divided equally between the two carbonyl oxygens O_I and O_{II} of Q_A^- (see Fig. 11).[6]

The parallel direction is the normal to the $d(x^2 - y^2)$ orbital and was calculated from the structural data as the normal to the best fitted plane containing N_1, N_2, N_3, and O_6 (see Figs. 6 and 10). The angle between this direction and the line connecting the metal ion and the center of Q_A is 30°. Substituting the values $d = -0.010$ K and $\theta = 30°$ in Eq. 20 we determine a value of $\langle R^3\rangle^{1/3} = 8.4$ Å, which is to be compared with the value of $\langle R^3\rangle^{1/3} = 10$ Å obtained from the structural data. This discrepancy suggests that the quinone ring is displaced when Q_A is reduced, as has been postulated by Allen et al. (1988).

[5]A larger anisotropic exchange interaction is expected (and in fact was observed by Butler et al., 1984) between Fe^{2+} and Q_A^- in native RCs. This is because of the closeness of higher excited orbital levels for Fe^{2+}.
[6]In fact, ENDOR experiments performed in RCs where the quinone oxygens O_I and O_{II} were replaced by ^{17}O show that the hyperfine coupling of these two oxygens are different ($A_I = 75$ MHz and $A_{II} = 94$ MHz) (Feher et al., 1985; Lubitz et al., 1985). It is found that about 44% of the unpaired electron density is on O_I (the side of the quinone closer to the metal ion) and 56% is on O_{II} (Lubitz, private communication). This result does not change significantly the value obtained for $\langle R^3\rangle^{1/3}$.

The dashed lines in Fig. 11 show the displaced position of Q_A^- that is consistent with the value of d.

REFERENCES

Abragam, A., and B. Bleaney. 1970. Electron Paramagnetic Resonance of Transition Ions. Clarendon Press, Oxford. 167–178, 455–466, 491–520.

Allen, J. P., G. Feher, T. O. Yeates, H. Komiya, and D. C. Rees. 1987. Structure of the reaction center from *Rhodobacter sphaeroides* R-26: the cofactors. *Proc. Natl. Acad. Sci. USA.* 84:5730–5734.

Allen, J. P., G. Feher, T. O. Yeates, H. Komiya, and D. C. Rees. 1988. Structure of the reaction center from *Rhodobacter sphaeroides* R-26: protein-cofactor (Quinones and Fe^{2+}) interactions. *Proc. Natl. Acad. Sci. USA.* 85:8487–8491.

Allen, J. P., E. J. Lous, R. A. Isaacson, M. Y. Okamura, and G. Feher. 1989. EPR and ENDOR Studies of $D^+Q_AFe^{2+}Q_B^-$ in Single Crystals of RCs from *Rb. sphaeroides. Biophys. J.* 55:222a (Abstr.)

Anderson, P. W. 1954. A mathematical model for the narrowing of spectral lines by exchange and motion. *J. Phys. Soc. Jap.* 9:316–339.

Anderson, P. W. 1959. New approach to the theory of superexchange interactions. *Phys. Rev.* 115:2–13.

Anderson, P. W., and P. R. Weiss. 1953. Exchange narrowing in paramagnetic resonance. *Rev. Mod. Phys.* 25:269–276.

Belford, R. L., and M. J. Nilges. 1979. Computer simulation of powder spectra. *EPR Symposium, 21st Rocky Mountain Conference, Denver, Colorado.* 21:179.

Boso, B., P. G. Debrunner, M. Y. Okamura, and G. Feher. 1981. Mössbauer spectroscopy studies of reaction centers from *Rhodopseudomonas sphaeroides* R-26. *Biochim. Biophys. Acta.* 638:173–177.

Brill, A. S. 1977. Transition Metal Ions in Biochemistry. Springer Verlag, Berlin. 40–70.

Buchanan, S. K., and G. C. Dismukes. 1987. Substitution of Cu^{2+} in the reaction center diquinone electron acceptor complex of *Rhodobacter sphaeroides*: determination of the metal-ligand coordination. *Biochemistry.* 26:5049–5055.

Bunker, G., E. A. Stern, R. E. Blankenship, and W. W. Parson. 1982. An X-ray absorption study of the iron site in bacterial photosynthetic reaction centers. *Biophys. J.* 37:539–551.

Butler, W. F., D. C. Johnston, H. B. Shore, D. R. Fredkin, M.Y. Okamura, and G. Feher. 1980. The electronic structure of Fe^{2+} in reaction centers from *Rhodopseudomonas sphaeroides.* I. Static magnetization measurements. *Biophys. J.* 32:967–992.

Butler, W. F., R. Calvo, D. R. Fredkin, R. A. Isaacson, M. Y. Okamura, and G. Feher. 1984. The electronic structure of Fe^{2+} in reaction

centers from *Rhodopseudomonas sphaeroides.* III. EPR measurements of the reduced acceptor complex. *Biophys. J.* 45:947–973.

Calvo, R., W. F. Butler, R. A. Isaacson, M. Y. Okamura, D. R. Fredkin, and G. Feher. 1982. Spin-lattice relaxation time of the reduced primary quinone in RCs from *Rhodopseudomonas sphaeroides:* determination of the zero field splitting of Fe^{2+}. *Biophys. J.* 37:111a (Abstr.)

Calvo, R., M. Passeggi, R. A. Isaacson, M. Y. Okamura, and G. Feher. 1989. The exchange interaction between Cu^{2+} and Q_A^- in reaction centers from *Rb. sphaeroides* R-26 in which Fe^{2+} has been replaced by Cu^{2+}. *Biophys. J.* 55:221a (Abstr.)

Coffman, R. E., and G. R. Buettner. 1979. A limit function for long range ferromagnetic and antiferromagnetic superexchange. *J. Phys. Chem.* 83:2387–2392.

Cotton, D. C. 1963. Chemical Applications of Group Theory. Wiley, New York. 31–49.

Cotton, F. A., and G. Wilkinson. 1980. Advanced Inorganic Chemistry. 4th ed. Wiley, New York. 752–758, 811–818.

Debrunner, P. G., C. E. Schula, G. Feher, and M. Y. Okamura. 1975. Mössbauer study of reaction centers from *Rhodopseudomonas sphaeroides. Biophys. J.* 15:226a (Abstr.)

Debus, R. J. 1985. The photosynthetic reaction center from *Rhodopseudomonas sphaeroides* R26.1: Influence of the H subunit and the Fe^{2+} on electron transfer. Ph.D. thesis. University of California at San Diego, La Jolla, California. 59–61.

Debus, R. J., G. Feher, and M. Y. Okamura. 1986. Iron-depleted reaction centers from *Rhodopseudomonas sphaeroides* R-26.1: characterization and reconstitution with Fe^{2+}, Mn^{2+}, Co^{2+}, Ni^{2+}, Cu^{2+}, and Zn^{2+}. *Biochemistry.* 25:2276–2287.

DeVault, D. 1984. Quantum Mechanical Tunneling in Biological Systems. Cambridge University Press, London. 119–121.

Dismukes, G. C., H. A. Frank, R. Friesner, and K. Sauer. 1984. Electronic interactions between iron and the bound semiquinones in bacterial photosynthesis. EPR spectroscopy of oriented cells of *Rhodopseudomonas viridis. Biochim. Biophys. Acta.* 764:253–271.

Dutton, P. L., J. S. Leigh, and D. W. Reed. 1973. Primary events in the photosynthetic reaction centers from *Rhodopseudomonas sphaeroides* strain R-26: triplet and oxidized states of bacteriochlorophyll and the identification of the primary acceptor. *Biochim. Biophys. Acta.* 292:654–664.

Eisenberger, P., M. Y. Okamura, and G. Feher. 1982. The electronic structure of Fe^{2+} in reaction centers from *Rb. sphaeroides.* II. Extended X-ray fine structure studies. *Biophysical J.* 37:523–538.

Evelo, R. G., H. M. Nan, and A. J. Hoff. 1988. A single-crystal EPR study of the reduced iron-quinone acceptor complex in reaction centers of *Rhodopseudomonas viridis. FEBS (Fed. Eur. Biochem. Soc.) Let.* 239:351–357.

Feher, G. 1957. Sensitivity considerations in microwave paramagnetic resonance absorption techniques. *Bell Syst. Tech. J.* 36:449–484.

Feher, G. 1971. Some chemical and physical properties of a bacterial reaction center particle and its primary photochemical reactants. *Photochem. Photobiol.* 14:373–388.

Feher, G., and M. Y. Okamura. 1978. Chemical composition and properties of reaction centers. *In* The Photosynthetic Bacteria. R. K. Clayton and W. R. Sistrom, editors. Plenum Press, New York. 349–386.

Feher, G., M. Y. Okamura, and J. D. McElroy. 1972. Identification of an electron acceptor in reaction centers of *Rhodopseudomonas sphaeroides* by EPR spectroscopy. *Biochim. Biophys. Acta.* 267:222–226.

Feher, G., R. A. Isaacson, M. Y. Okamura, and W. Lubitz. 1985. Electron nuclear double resonances of semiquinones in RCs from *Rhodopseudomonas sphaeroides. In* Antennas and Reaction Centers of Photosynthetic Bacteria. Springer Series in Chemical Physics. M. E. Michel-Beyerle, editor. Springer-Verlag, Berlin. 42:174–189.

Feher, G., R. A. Isaacson, R. Debus, and M. Y. Okamura. 1986. The superhyperfine structure of ^{14}N in iron depleted RCs from *Rb. sphaeroides* R26.1 reconstituted with ^{65}Cu: Determination of the number of nitrogen to metal ligands. *Biophys. J.* 49:585a (Abstr.)

Froncisz, W., and J. S. Hyde. 1980. Broadening by strains of lines in the g-parallel region of Cu^{2+} EPR spectra. *J. Chem. Phys.* 73:3123–3131.

Gast, P., A. Gottschalk, J. R. Norris, and G. L. Closs. 1989. Orientation dependence of the EPR signal from the reduced iron-quinone complex in single crystal of the reaction center protein from *Rhodopseudomonas viridis. FEBS (Fed. Eur. Biochem. Soc.) Lett.* 243:1–4.

Gray, H. B., and E. I. Solomon. 1981. Electronic structures of blue copper centers in proteins. *In* Copper Proteins. T. G. Spiro, editor. John Wiley and Sons, Inc., New York. 3:1–39.

Hay, P. J., J. C. Thibeault, and R. Hoffmann. 1975. Orbital interactions in metal dimer complexes. *J. Am. Chem. Soc.* 97:4884–4899.

Hoff, A. J. 1979. Applications of ESR to photosynthesis. *Phys. Reports.* 54:75–200.

Hoff, A. J. 1987. Electron paramagnetic resonance in photosynthesis. *In* Photosynthesis. J. Amesz, editor. Elsevier, Amsterdam. 97–123.

Hyde, J. S., and W. Froncisz. 1982. The role of microwave frequency in EPR spectroscopy of copper complexes. *Ann. Rev. Biophys. Bioeng.* 11:391–417.

Kanamori, J. 1963. Anisotropy and magnetostriction of ferromagnetic and antiferromagnetic materials. *In* Magnetism. G. T. Rado and H. Suhl, editors. New York. 127–203.

Kokoszka, G. F., and G. Gordon. 1969. Metal–metal exchange interactions. *In* Transition Metal Chemistry. R. Carlin, editor. Marcel Dekker, New York.

Leigh, J. S., and P. L. Dutton. 1972. The primary electron acceptor in photosynthesis. *Biochem. Biophys. Res. Commun.* 46:414–421.

Levstein, P., and R. Calvo. 1990. Superexchange coupling mediated by carboxylate and hydrogen bridges in copper-amino acid complexes. *Inorg. Chem.* In press.

Lubitz, W., E. C. Abresch, R. J. Debus, R. A. Isaacson, M. Y. Okamura, and G. Feher. 1985. Electron nuclear double resonance of semiquinones in reaction centers of *Rhodopseudomonas sphaeroides. Biochim. Biophys. Acta.* 808:464–469.

Maki, A. H., and B. R. McGarvey. 1958a. Electron spin resonance in transition metal chelates. I. Copper (II) bis Acetylacetonate. *J. Chem. Phys.* 29:31–34.

Maki, A. H., and B. R. McGarvey. 1958b. Electron spin resonance in transition metal chelates. II Copper (II) bis-salicylaldehyde-imine. *J. Chem. Phys.* 29:35–38.

McElroy, J. D., G. Feher, and D. Mauzerall. 1970. Observation of a second light induced EPR signal from reaction centers of photosynthetic bacteria. *Biophys. Soc. Annu. Meet. Abstr.* 10:204a (Abstr.)

McElroy, J. D., D. C. Mauzerall, and G. Feher. 1974. Characterization of primary reactants in bacterial photosynthesis II. Kinetic studies of the light-induced signal ($g = 2.0026$) and the optical absorbance changes at cryogenic temperatures. *Biochim. Biophys. Acta.* 333:261–278.

Mims, W. B., and J. Peisach, 1989. ESEEM and LEFE of metalloproteins and model compounds. *In* Advanced EPR, Applications in Biology and Biochemistry. A. J. Hoff, editor. Elsevier, Amsterdam. 1–57.

Moriya, T. 1960. Anisotropic superexchange interaction and weak ferromagnetism. *Phys. Rev.* 120:91–98.

Okamura, M. Y., and G. Feher. 1989. Superexchange mechanism of electron transfer from Q_A^- to Q_B in the Fe-quinone complex of bacterial reaction centers. *Biophys. J.* 55:221a (Abstr.)

Okamura, M. Y., R. A. Isaacson, and G. Feher. 1975. The primary acceptor in bacterial photosynthesis: the obligatory role of ubiquinone in photoactive reaction centers of *Rhodopseudomonas sphaeroides. Proc. Natl. Acad. Sci. USA.* 72:3491–3495.

Okamura, M. Y., D. R. Fredkin, R. A. Isaacson, and G. Feher. 1979. Magnetic interactions and electron transfer kinetics of the reduced intermediate acceptor in reaction centers (RCs) of *Rhodopseudomonas sphaeroides* R-26. Evidence for thermally induced tunneling. *In* Tunneling in Biological Systems. B. Chance, D. C. DeVault, H. Fraunenfelder, R. A. Marcus, J. R. Schrieffer, and N. Sutin, editors. Academic Press, New York. 729–743.

Okamura, M. Y., G. Feher, and N. Nelson. 1982. Reaction centers. *In* Photosynthesis: Energy Conversion by Plants and Bacteria. Govindjee, editor. Academic Press, New York. 1:195–272.

Rothenberger, K. S. 1988. Part I: Determination of quadripole couplings via L band B_0IIB_1, electron paramagnetic resonance. Ph.D. thesis. University of Illinois, Urbana, Illinois. 98–270, 389–558.

Schweiger, A. 1982. Electron Nuclear Double Resonance of Transition Metal Complexes with Organic Ligands, Structure and Bonding. Springer-Verlag, Berlin. 51:71–75.

Slichter, C. 1980. The Principles of Magnetic Resonance. Springer-Verlag, Berlin. 56–62.

Solomon, E. I., K. W. Penfield, and D. E. Wilcox. 1983. Active sites in copper proteins. An electronic structure overview. *In* Structure and Bonding. M. J. Clarke, J. B. Goodenough, J. A. Ibers, C. K. Jorgensen, J. B. Neilands, D. Reinen, R. Weiss, and R. J. P. Williams, editors. Springer-Verlag, Berlin. 53:1–57.

Steren, C. A., R. Calvo, O. E. Piro, and B. E. Rivero. 1989. Molecular Structure of bis-L-Leucinato Zinc(II) and Single Crystal EPR Spectra of Substitutionally ^{63}Cu Doped. Complex. *Inorg. Chem.* 28:1933–1938.

Van Camp, H. L., R. H. Sands, and J. A. Fee. 1982. An examination of the cyanide derivative of bovine superoxide dismutase with electron-nuclear double resonance. *Biochim. Biophys. Acta.* 704:75–89.

Zeiger, H. J., and G. W. Pratt. 1973. Magnetic Interactions in Solids. Clarendon Press, Oxford. 103–197.